

Cite this: *Dalton Trans.*, 2022, **51**, 4338

Oxygenolysis of a series of copper(II)-flavonolate adducts varying the electronic factors on supporting ligands as a mimic of quercetin 2,4-dioxygenase-like activity†

Nirmalya Podder,  Subhasis Dey, Anakuthil Anoop * and Sukanta Mandal *

Four copper(II)-flavonolate compounds of type $[\text{Cu}(\text{L}^{\text{R}})(\text{fla})]$ {where $\text{L}^{\text{R}} = 2-(p\text{-R-benzyl(dipyridin-2-ylmethyl)amino)acetate}$; $\text{R} = -\text{OMe}$ (**1**), $-\text{H}$ (**2**), $-\text{Cl}$ (**3**) and $-\text{NO}_2$ (**4**)} have been developed as a structural and functional enzyme–substrate (ES) model of the Cu^{2+} -containing quercetin 2,4-dioxygenase enzyme. The ES model complexes **1–4** are synthesized by reacting 3-hydroxyflavone in the presence of a base with the respective acetate-bound copper(II) complexes, $[\text{Cu}(\text{L}^{\text{R}})(\text{OAc})]$. In the presence of dioxygen the ES model complexes undergo enzyme-type oxygenolysis of flavonolate (dioxygenase type bond cleavage reaction) at 80 °C in DMF. The reactivity shows a substituent group dependent order as $-\text{OMe}$ (**1**) > $-\text{H}$ (**2**) > $-\text{Cl}$ (**3**) > $-\text{NO}_2$ (**4**). Experimental and theoretical studies suggest a single-electron transfer (SET) from flavonolate to dioxygen, rather than valence tautomerism $\{[\text{Cu}^{\text{II}}(\text{fla}^-)] \leftrightarrow [\text{Cu}^{\text{I}}(\text{fla}^{\cdot})]\}$, to generate the reactive flavonoxy radical (fla $^{\cdot}$) that reacts further with the superoxide radical to bring about the oxygenative ring opening reaction. The SET pathway has been further verified by studying the dioxygenation reaction with a redox-inactive Zn^{2+} complex, $[\text{Zn}(\text{L}^{\text{OMe}})(\text{fla})]$ (**5**).

Received 9th December 2021,
Accepted 7th February 2022

DOI: 10.1039/d1dt04151g

rsc.li/dalton

Introduction

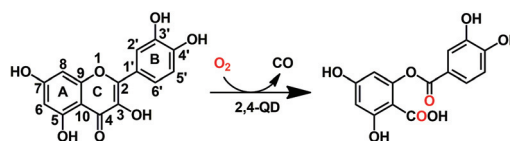
Quercetin 2,4-dioxygenases (2,4-QDs), found in soil microorganisms, catalyze the cleavage of two carbon–carbon bonds of quercetin (3',4',5,7-tetrahydroxyflavonol) in an oxygenative ring-opening reaction *via* activation of molecular dioxygen to yield the corresponding phenolic carboxylic acid esters (depside) and carbon monoxide (Scheme 1).¹

The natural fungal 2,4-QDs are highly glycosylated bicupin proteins, containing a type II copper ion at the active site. The X-ray crystal structure of the enzyme from *Aspergillus japonicus*^{2,3} and the EPR spectroscopic investigations revealed two coordination forms of the copper ion.^{4,5} In one form (*minor* conformation 30%) the copper(II) ion is ligated with three histidine imidazoles (His-66, His-68, and His-112), one water molecule and a carboxylate group of Glu-73 in a distorted trigonal bipyramidal/square pyramidal fashion. In the other form (*major* conformation 70%) the copper ion adopts a distorted tetrahedral geometry with three histidine residues and a

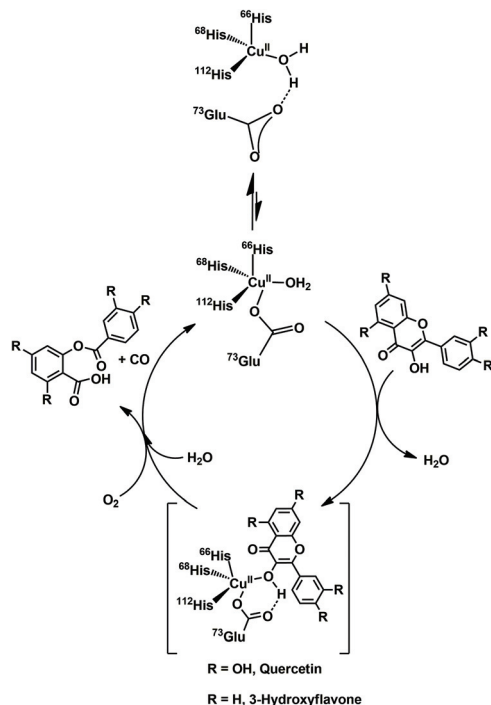
water molecule without the direct coordinative interaction with the glutamate group. In the major conformation the glutamate residue is involved in hydrogen bonding interaction with the coordinated water molecule. In the enzymatic reaction it is proposed that at the first step substrate quercetin binds to the copper(II) ion through the deprotonated 3-hydroxy group of flavonolate by replacing the water molecule, forming an enzyme–substrate (ES) complex with a distorted square pyramidal geometry under anaerobic conditions.⁴ In the next step dioxygenation of the substrate takes place under aerobic conditions at the ES complex *via* the dioxygen activation pathway to form the depside with the concomitant production of CO (Scheme 2).³ The carboxylate group of Glu73 plays an important role in the enzymatic reaction. In the absence of Glu-73 the enzyme lost the activity,^{2,4} indicating that the carboxylate coordination to the native active site plays a crucial role in the catalytic activity. The intriguing role of the carboxylate moiety is not understood yet clearly. It is presumed that the glutamate moiety may facili-

Department of Chemistry, Indian Institute of Technology Kharagpur,
Kharagpur-721302, India. E-mail: sukanta.mandal@chem.iitkgp.ac.in,
anoop@chem.iitkgp.ac.in

† Electronic supplementary information (ESI) available. CCDC 2112719, 2112720, 2112721, 2112723, 2112724, 2112725, 2112726 and 2112727. For ESI and crystallographic data in CIF or other electronic format see DOI: 10.1039/d1dt04151g



Scheme 1



Scheme 2

tate the reaction in various ways, such as (i) it may act as a base to deprotonate the substrate, (ii) it may stabilize the ES adduct *via* hydrogen bonding interaction, and (iii) it may finely tune the redox potential of the metal ion in the ES adduct to reduce the energy barrier for dioxygen activation.^{2,5}

In the literature, several biomimetic structural and functional models of 2,4-QD dealt with Cu(II)^{6–11} and other transition metal complexes (Mn, Fe, Co, Ni *etc.*)^{12–19} have been reported. In the biomimetic study, the pivotal role of the carboxylate moiety in the dioxygenation reactivity of quercetinase was nicely demonstrated by Speier and co-workers with flavonolate bound ES-model complex [Cu^{II}(fla)(idpa)](ClO₄) (idpa: 3,3'-iminobis(*N,N*-dimethylpropylamine); fla: flavonolate).⁹ It was found that the oxygenative degradation of the bound flavonolate substrate in the [Cu^{II}(fla)(idpa)](ClO₄) complex was promoted dramatically in the presence of excess acetate ions. It is believed that acetate binds with the copper centre and compels to change the bidentate chelating binding mode of flavonolate to monodentate. This results in an increase of the electron density in the substrate, thus accelerating its reactivity towards dioxygen. With this observation of the rate-enhancing effect of the carboxylate co-ligand, later on a few model complexes containing copper ions have been synthesized by designing ligands having three nitrogen and one carboxylate oxygen donor group keeping in mind the active site coordination environment of the minor form of 2,4-QD.^{10,11,13}

However, anomalous reactivity trends were observed with various model complexes. For instance, with copper(II) complex [Cu(L)(Cl)] (L: 1-benzyl-4-acetato-1,4,7-triazacyclononane) no outstanding effect on reactivity due to the presence

of the carboxylate group was observed.¹⁰ In fact, a much elevated temperature (~100 °C) was required to induce the oxygenation of the substrate. Moreover, formations of the non-enzymatic products were observed. On the other hand with the copper(II) ES complex, [Cu^{II}(L)(fla)], (HL: 2-[[bis(pyridin-2-ylmethyl)amino]methyl]benzoic acid) moderate enzymatic activity at a comparatively lower temperature (~70 °C) was reported.¹³ In recent studies Sun and Itoh *et al.* demonstrated different reactivities in the dioxygenation of bound flavonolate at 75–90 °C with a series of copper(II) complexes supported by carboxylate-containing (pyridylalkyl)amine ligands.¹¹ It was found that the extent of interaction (strong or weak) of the carboxylate group with the copper centre and the size of the chelate ring finely control the reactivity by tuning the Lewis acidity of the copper(II) ion. Thus, from the above literature reports, it is evident that the mere presence of the carboxylate group does not exclusively increase the reaction rate; rather the overall electronic effects exerted by the surrounding ligand finely tune the reactivity. This opens a door to study further the influence of electronic factors on reactivity by designing ligands with systematic variation in their electronic properties. With this purpose we focus our study on the electronic substituent effects of the supporting model ligand of the Cu(II) ES adduct on their quercetinase-like activity. Herein we report the synthesis and characterization of a set of acetate bound copper (II) complexes [Cu^{II}(L^R)(OAc)] {R = -OMe (**I**), -H (**II**), -Cl (**III**), and -NO₂ (**IV**)} and their flavonolate adducts [Cu^{II}(L^R)(fla)] {R = -OMe (**1**), -H (**2**), -Cl (**3**), and -NO₂ (**4**)} supported by the carboxylate-containing tetradentate N₃O donor ligand L^R (where LiL^R = lithium 2-(*p*-R-benzyl(dipyridin-2-ylmethyl)amino)acetate; R = -OMe, -H, -Cl, and -NO₂) (Fig. 1). The reactivity towards dioxygenation with all flavonolate adducts **1–4** has been investigated for single-turnover at 80 °C in *N,N*-dimethyl-

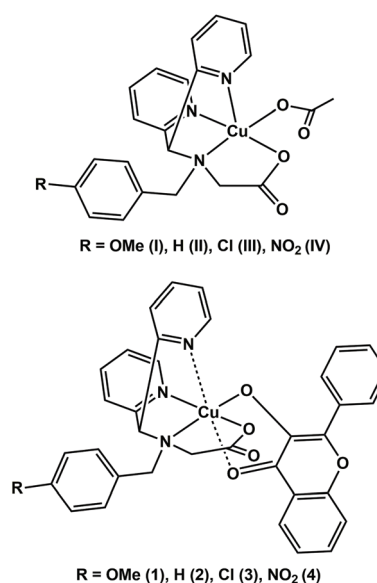


Fig. 1 Acetate-bound and flavonolate-bound copper(II) complexes considered in this work.

formamide (DMF) medium. All complexes show enzyme-type reactivity. The complexes exhibit substituent group dependent reactivities, where a higher rate has been observed with an electron donating substituent group. A linear Hammett correlation of the substituent groups with the rate of reactions is observed. A single-electron transfer (SET) pathway from flavonolate to dioxygen, rather than valence tautomerism $\{[Cu^{II}(fla^-)] \leftrightarrow [Cu^I(fla^{\cdot})]\}$, has been proposed to generate a reactive flavonoxyl radical (fla^{\cdot}) that reacts further with the superoxide radical to bring about the oxygenative degradation reaction. The SET pathway has been verified by studying the dioxygenation reaction with a redox-inactive Zn^{2+} complex, $[Zn(L^{OMe})(fla)]$ (5). Further DFT calculations are performed with complex 2 to elucidate the plausible reaction pathway.

Experimental section

Materials and reagents

All required chemicals except the ligands, and $Cu(II)$ and $Zn(II)$ complexes were purchased from commercial sources such as Sigma Aldrich, Alfa Aesar, TCI Chemicals (India) Pvt. Ltd. and Sisco Research Laboratories Pvt. Ltd (SRL) India, and were used without further purification. Organic solvents were dried/purified prior to use. Di-2-pyridylmethanamine was prepared following the literature procedure.²⁰

Synthesis of ligands

All four ligands L^R ($R = -OMe, -H, -Cl,$ and $-NO_2$) were isolated as their lithium salts. The three ligands LiL^R ($R = -OMe, -H,$ and $-Cl$) were synthesized following a similar synthetic procedure; whereas the ligand LiL^{NO_2} was synthesized by a different synthetic route.

General synthetic procedure of ligands LiL^R ($R = -OMe, -H,$ and $-Cl$)

The synthetic strategy comprises the following three steps:

Step 1: general synthesis of *N*-(*p*-*R*-benzyl)-1,1-di(pyridin-2-yl)methanamine (Py_2NBz^R). *p*-Methoxybenzaldehyde or benzaldehyde or *p*-chlorobenzaldehyde (8.97 mmol) was added slowly to a solution of di-2-pyridylmethanamine (1.66 g, 8.97 mmol) in dry ethanol (20 mL). After stirring for 24 hours at room temperature the solvent from each reaction solution was removed completely under reduced pressure. The thick oily residue obtained from each reaction was then dissolved in methanol (20 mL) and warmed at 45 °C in an oil bath. In each solution, an excess of $NaBH_4$ (1.36 g, 35.88 mmol) was added portion wise over a period of one hour and the solution was stirred for another 24 hours at 45 °C. After evaporation of the solvent completely, each residue was treated with an aqueous brine solution and the corresponding reduced product was extracted with CH_2Cl_2 (5×50 mL). The combined organic layers were then washed with a saturated brine solution and dried over anhydrous $MgSO_4$. Filtration followed by removal of the solvent yielded the respective product (Py_2NBz^{OMe} or

Py_2NBz^H or Py_2NBz^{Cl}) as reddish-brown oil. The yields and the 1H NMR data of the three products are presented below.

N-(*p*-Methoxybenzyl)-1,1-di(pyridin-2-yl)methanamine (Py_2NBz^{OMe}). Yield: 2.35 g, 86%. 1H NMR (400 MHz, $CDCl_3$, 300 K): δ (ppm) 8.58 (d, 2H), 7.64 (2H), 7.45 (d, 2H), 7.30 (2H), 7.16 (2H), 6.86 (d, 2H), 5.19 (s, 1H), 3.79 (s, 5H), 1.88 (br. s, NH).

N-Benzyl-1,1-di(pyridin-2-yl)methanamine (Py_2NBz^H). Yield: 2.07 g, 84%. 1H NMR (400 MHz, $CDCl_3$, 300 K): δ (ppm) 8.57 (d, 2H), 7.63 (t, 2H), 7.44 (d, 2H), 7.35–7.23 (m, 5H), 7.16–7.13 (m, 2H), 5.12 (s, 1H), 3.78 (s, 2H), 2.07 (br. s, NH).

N-(*p*-Chlorobenzyl)-1,1-di(pyridin-2-yl)methanamine (Py_2NBz^{Cl}). Yield: 1.80 g, 65%. 1H NMR (400 MHz, $CDCl_3$, 300 K): δ (ppm) 8.62 (d, 2H), 7.73 (t, 2H), 7.52 (m, 6H), 7.35 (d, 2H), 5.62 (s, 1H), 4.10 (s, 2H), 2.06 (br. s, NH).

Step 2: general synthesis of ethyl 2-((di(pyridine-2-yl)methyl)(*p*-*R*-benzyl)amino)acetate ($Py_2NEtOAcBz^R$). A solution of Py_2NBz^{OMe} or Py_2NBz^H or Py_2NBz^{Cl} (3.30 mmol) in 20 mL of dry acetonitrile was taken in a 100 mL two necked round-bottom flask. To each solution K_2CO_3 (2.28 g, 16.50 mmol) and a catalytic amount of KI were added as a solid, and the reaction vessel was flushed with dinitrogen. A solution of ethyl 2-chloroacetate (0.60 g, 4.90 mmol) in 10 mL of acetonitrile was then added slowly to each reaction mixture under stirring conditions. Afterwards all three reaction mixtures were refluxed under a dinitrogen atmosphere for 72 hours. After cooling to room temperature, the individual reaction mixture was filtered through Celite to remove the white solid residues. The solvent was completely removed from each filtrate under reduced pressure. Dichloromethane (50 mL) was added to the respective residue, and it was washed thrice with brine solution. Evaporation of the dichloromethane fraction afforded the respective crude product as brown oil. The pure product in each case was obtained by column chromatography on silica using $CH_2Cl_2/MeOH$ (ratio varied from 1:0 to 20:1) as an eluent. The yield and 1H NMR data of each product at step 2 are reported below.

Ethyl 2-((di(pyridine-2-yl)methyl)(*p*-methoxybenzyl)amino)acetate ($Py_2NEtOAcBz^{OMe}$). Yield: 0.98 g, 76%. 1H NMR (400 MHz, $CDCl_3$, 300 K): δ (ppm) 8.54 (d, 2H), 7.76 (d, 2H), 7.67 (t, 2H), 7.34 (d, 2H), 7.13 (t, 2H), 6.84 (d, 2H), 5.49 (s, 1H), 4.09 (q, 2H), 3.79 (s, 5H), 3.35 (s, 2H), 1.20 (t, 3H).

Ethyl 2-((di(pyridine-2-yl)methyl)(benzyl)amino)acetate ($Py_2NEtOAcBz^H$). Yield: 0.86 g, 72%. 1H NMR (400 MHz, $CDCl_3$, 300 K): δ (ppm) 8.55 (d, 2H), 7.77 (d, 2H), 7.67 (t, 2H), 7.43 (d, 2H), 7.33–7.23 (m, 3H), 7.15–7.12 (m, 2H), 5.52 (s, 1H), 4.06 (q, 2H), 3.86 (s, 2H), 3.37 (s, 2H), 1.21 (t, 3H).

Ethyl 2-((di(pyridine-2-yl)methyl)(*p*-chlorobenzyl)amino)acetate ($Py_2NEtOAcBz^{Cl}$). Yield: 0.76 g, 58%. 1H NMR (400 MHz, $CDCl_3$, 300 K): δ (ppm) 8.55 (d, 2H), 7.72–7.64 (m, 4H), 7.37 (d, 2H), 7.28 (d, 2H), 7.14 (m, 2H), 5.48 (s, 1H), 4.09 (q, 2H), 3.83 (s, 2H), 3.35 (s, 2H), 1.21 (t, 3H).

Step 3: general synthesis of lithium 2-(*p*-*R*-benzyl(dipyridin-2-ylmethyl)amino)acetate (LiL^R). $Py_2NEtOAcBz^{OMe}$ or $Py_2NEtOAcBz^H$ or $Py_2NEtOAcBz^{Cl}$ (2.01 mmol) was treated with $LiOH \cdot H_2O$ (0.42 g, 10.02 mmol) in methanol (15 mL) and stirred for 24 hours at room temperature. After that the metha-

nol solvent was removed completely from each solution under reduced pressure. Dichloromethane (20 mL) was then added to each residue, and the mixture was stirred for another one hour. Filtration and evaporation of the solvent yielded the respective lithium salt of the ligand in pure form as a yellow solid. The yields and characterization data of the three ligands are reported below.

Lithium 2-(*p*-methoxybenzyl(dipyridin-2-ylmethyl)amino)acetate (LiL^{OMe}). Yield: 0.72 g, 97%. HRMS-ESI(+) (in MeOH with a trace quantity of HCOOH): *m/z* 364.1650 (calculated for C₂₁H₂₂N₃O₃ {HL^{OMe} + H⁺}⁺; *m/z* 364.1661); *m/z* 418.0838 (calculated for C₂₂H₂₅N₃NaO₄ {HL^{OMe} + CH₃OH + Na⁺}⁺; *m/z* 418.1743). ATR-FTIR (cm⁻¹, solid sample, selected bands): 1608 (s), 1590 (s), 1571 (w) ($\nu_{\text{asym}}(\text{COO})$); 1466 (m), 1433 (s), 1402 (s) ($\nu_{\text{sym}}(\text{COO})$). ¹H NMR (400 MHz, CD₃OD, 300 K): δ (ppm) 8.48 (d, 2H), 7.79 (m, 4H), 7.26 (m, 4H), 6.85 (d, 2H), 5.42 (s, 1H), 3.76 (s, 3H), 3.71 (s, 2H), 3.02 (s, 2H).

Lithium 2-(benzyl(dipyridin-2-ylmethyl)amino)acetate (LiL^H). Yield: 0.65 g, 95%. HRMS-ESI(+) (in MeOH with a trace quantity of HCOOH): *m/z* 276.1484 (calculated for C₁₈H₁₈N₃ {HL^H - CH₂CO₂H + 2H⁺}⁺; *m/z* 276.1501); *m/z* 388.0736 (calculated for C₂₁H₂₃N₃NaO₃ {HL^H + CH₃OH + Na⁺}⁺; *m/z* 388.1637); *m/z* 334.1535 (calculated for C₂₀H₂₀N₃O₂ {HL^H + H⁺}⁺; *m/z* 334.1556). ATR-FTIR (cm⁻¹, solid sample, selected bands): 1615 (w), 1591 (s), 1570 (w) ($\nu_{\text{asym}}(\text{COO})$); 1468 (m), 1434 (s), 1403 (s) ($\nu_{\text{sym}}(\text{COO})$). ¹H NMR (400 MHz, CD₃OD, 300 K): δ (ppm) 8.46 (d, 2H), 7.80 (m, 4H), 7.38–7.26 (m, 7H), 5.52 (s, 1H), 3.82 (s, 2H), 3.05 (s, 2H).

Lithium 2-(*p*-chlorobenzyl(dipyridin-2-ylmethyl)amino)acetate (LiL^{Cl}). Yield: 0.70 g, 93%. HRMS-ESI(+) (in MeOH with a trace quantity of HCOOH): *m/z* 392.2003 (calculated for C₂₀H₂₀ClLiN₃O₃ {LiL^{Cl} + H₂O + H⁺}⁺; *m/z* 392.1353); *m/z* 414.1788 (calculated for C₂₀H₁₉ClLiN₃NaO₃ {LiL^{Cl} + H₂O + Na⁺}⁺; *m/z* 414.1173). ATR-FTIR (cm⁻¹, solid sample, selected bands): 1592 (s), 1573 (s) ($\nu_{\text{asym}}(\text{COO})$); 1437 (s), 1410 (s) ($\nu_{\text{sym}}(\text{COO})$). ¹H NMR (400 MHz, CD₃OD, 300 K): δ (ppm) 8.42 (d, 2H), 7.84 (d, 2H), 7.78 (t, 2H), 7.40 (d, 2H), 7.27–7.23 (m, 4H), 5.56 (s, 1H), 3.83 (s, 2H), 3.04 (s, 2H).

Synthetic procedure of ligand LiL^{NO₂}

The ligand was synthesized by following three steps.

Step 1: synthesis of ethyl 2-((di(pyridin-2-yl)methyl)amino)acetate (Py₂NEtOAc). Di-2-pyridylmethanamine (1.81 g, 9.77 mmol) was dissolved in dry tetrahydrofuran (THF) (50 mL) and the solution was cooled over an ice-bath. Into this precooled solution, a mixture of ethyl 2-chloroacetate (1.18 g, 9.63 mmol) and *N,N*-diisopropylethylamine (DIPEA) (2.30 mL, 13.20 mmol) in THF (50 mL) was added dropwise over a period of 30 minutes. After completion of addition of the reagents the reaction mixture was stirred in the ice bath overnight under a dinitrogen atmosphere. After filtration, the solvent was completely removed under reduced pressure. The acquired residue was dissolved in dichloromethane (CH₂Cl₂) (50 mL) and washed with aqueous NaHCO₃ (2 × 10 mL) followed by water (2 × 10 mL). After that the organic layer was dried over anhydrous MgSO₄. Filtration and evaporation of the

solvent yielded the crude product as brown oil. It was then purified by column chromatography on silica using CH₂Cl₂:MeOH (99:1, v/v) as an eluent to afford 1.14 g of the product as reddish brown oil (yield: 43%). ¹H NMR (400 MHz, CDCl₃, 300 K): δ (ppm) 8.55 (d, 2H), 7.62 (t, 2H), 7.43 (d, 2H), 7.14 (t, 2H), 5.13 (s, 1H), 4.16 (q, 2H), 3.43 (s, 2H), 2.12 (br. s, N-H), 1.23 (t, 3H).

Step 2: synthesis of ethyl 2-((di(pyridin-2-yl)methyl)(4-nitrobenzyl)amino)acetate (Py₂NEtOAcBz^{NO₂}). Py₂NEtOAc (0.90 g, 3.32 mmol), K₂CO₃ (2.30 g, 16.64 mmol) and a catalytic amount of KI were taken together in a 100 mL round bottom flask. It was then charged with 20 mL of acetonitrile and the reaction vessel was flushed with dinitrogen. To this an acetonitrile (15 mL) solution of 1-(chloromethyl)-4-nitrobenzene (0.57 g, 3.32 mmol) was added slowly under stirring conditions. After completion of addition, the reaction mixture was heated to reflux for 72 hours. After cooling to room temperature, the reaction mixture was filtered through Celite to separate out the solid particles. The solvent was then removed completely under reduced pressure. The organic residue was dissolved in 50 mL of CH₂Cl₂ and the solution was washed thrice with brine water. The product was purified by column chromatography on silica using CH₂Cl₂:MeOH (99:1, v/v) as an eluent to afford 0.74 g of the pure ligand as reddish brown oil (yield: 55%). ¹H NMR (400 MHz, CDCl₃, 300 K): δ (ppm) 8.55 (d, 2H), 8.15 (d, 2H), 7.67–7.62 (m, 6H), 7.15 (t, 2H), 5.49 (s, 1H), 4.08 (q, 2H), 3.99 (s, 2H), 3.39 (s, 2H), 1.19 (t, 3H).

Step 3: synthesis of lithium 2-((di(pyridin-2-yl)methyl)(4-nitrobenzyl)amino)acetate (LiL^{NO₂}). Treatment of Py₂NEtOAcBz^{NO₂} (0.70 g, 1.72 mmol) with LiOH·H₂O (0.37 g, 8.77 mmol) in methanol afforded the lithium salt of the ligand, LiL^{NO₂}, as a yellowish solid (yield: 0.60 g, 91%). HRMS-ESI(+) (in MeOH with a trace quantity of HCOOH): *m/z* 379.2201 (calculated for C₂₀H₁₉N₄O₄ {HL^{NO₂} + H⁺}⁺; *m/z* 379.1406). ATR-FTIR (cm⁻¹, solid sample, selected bands): 1611 (m) ($\nu_{\text{asym}}(\text{COO})$); 1537 (s) ($\nu_{\text{asym}}(\text{NO}_2)$), 1410 (w) ($\nu_{\text{sym}}(\text{COO})$), 1346 (s) ($\nu_{\text{sym}}(\text{NO}_2)$). ¹H NMR (400 MHz, CD₃OD, 300 K): δ (ppm) 8.44 (d, 2H), 8.14 (d, 2H), 7.83 (d, 2H), 7.77 (t, 2H), 7.69 (d, 2H), 7.25 (t, 2H), 5.60 (s, 1H), 3.98 (s, 2H), 3.09 (s, 2H).

Synthesis of acetate-bound copper(II) complexes [Cu(L^R)(OAc)]

The complexes were synthesized according to the following procedure. To a magnetically stirred solution of methanol (15 mL) containing LiL^R (1.40 mmol), a methanol solution (5 mL) of Cu(OAc)₂·H₂O (0.28 g, 1.40 mmol) was added dropwise. The reaction mixture was stirred under air at room temperature for 6 hours and then it was filtered to remove insoluble particles. The volume of the filtrate was reduced to about 4 mL by evaporating the solvent under reduced pressure. The compound was isolated as a powder by the addition of an excess of diethylether into the filtrate. Analytical grade compounds were obtained through recrystallization from methanol and diethylether. The single crystals suitable for the X-ray structural analysis of compounds **I**, **II**, **III** and **IV** were obtained by slow diffusion of diethylether into the methanol solutions of the complexes.

[Cu^{II}(L^{OMe})(OAc)]·2H₂O (I·2H₂O)

Yield: 0.45 g (62%). Color: blue. Anal. Calcd for C₂₃H₂₇CuN₃O₇: C 53.02, H 5.22, N 8.06. Found: C 53.08, H 5.01, N 8.16. HRMS-ESI(+) (in MeOH with a trace quantity of HCOOH): *m/z* 381.0924 (calculated for C₂₀H₂₀CuN₃O₅ {[Cu(L^{OMe})]⁺ - CO₂}⁺: *m/z* 381.0902); 471.0863 (calculated for C₂₂H₂₂CuN₃O₅ {[Cu(L^{OMe})(HCOO)] + H⁺}⁺: *m/z* 471.0855); 897.1586 (calculated for C₄₃H₄₃Cu₂N₆O₈ {2[Cu(L^{OMe})]⁺ + HCOOH + H⁺ + 2e⁻}⁺: *m/z* 897.1734). ATR-FTIR (cm⁻¹, solid sample, few selected bands): 3523 (m), 3433 (m), 3392 (m), 1609 (s), 1588 (s), 1516 (s), 1458 (w), 1440 (m), 1387 (w), 1370 (s), 1330 (s). UV-vis [*λ*_{max}, nm (ε, M⁻¹ cm⁻¹): (in MeOH) 686 (70), 305 (sh, 2150), 267 (7480), 258 (7563), 225 (14 530).

[Cu^{II}(L^H)(OAc)]·MeOH (II·MeOH)

Yield: 0.48 g (70%). Color: blue. Anal. Calcd for C₂₂H₂₃CuN₃O₅: C 56.72, H 5.17, N 8.63. Found: C 56.80, H 5.02, N 8.85. HRMS-ESI(+) (in MeOH with a trace quantity of HCOOH): *m/z* 351.0814 (calculated for C₁₉H₁₈CuN₃ {[Cu(L^H)]⁺ - CO₂}⁺: *m/z* 351.0797); 835.1383 (calculated for C₄₁H₃₇Cu₂N₆O₆ {2[Cu(L^H)]⁺ + HCOO⁻}⁺: *m/z* 835.1367). ATR-FTIR (cm⁻¹, solid sample, few selected bands): 3494 (br), 3453 (br), 1609 (s), 1595 (s), 1455 (m), 1443 (m), 1376 (m), 1353 (m), 1332 (s). UV-vis [*λ*_{max}, nm (ε, M⁻¹ cm⁻¹): (in MeOH) 708 (80), 610 (sh, 60), 305 (sh, 2490), 267 (7920), 258 (8365), 206 (20 530).

[Cu^{II}(L^{Cl})(OAc)]·2H₂O (III·2H₂O)

Yield: 0.56 g (76%). Color: blue. Anal. Calcd for C₂₂H₂₄ClCuN₃O₆: C 50.29, H 4.60, N 8.00. Found: C 50.22, H 4.45, N 7.92. HRMS-ESI(+) (in MeOH with a trace quantity of HCOOH): *m/z* 385.0418 (calculated for C₁₉H₁₇ClCuN₃ {[Cu(L^{Cl})]⁺ - CO₂}⁺: *m/z* 385.0407); 475.0367 (calculated for C₂₁H₁₉ClCuN₃O₄ {[Cu(L^{Cl})(HCOO)] + H⁺}⁺: *m/z* 475.0360); 905.0587 (calculated for C₄₁H₃₇Cl₂Cu₂N₆O₆ {2[Cu(L^{Cl})]⁺ + HCOOH + H⁺ + 2e⁻}⁺: *m/z* 905.0744). ATR-FTIR (cm⁻¹, solid sample, few selected bands): 3509 (m), 3439 (m), 3402 (m), 1623 (s), 1609 (s), 1595 (s), 1496 (w), 1442 (m), 1388 (w), 1372 (s), 1355 (w), 1334 (s). UV-vis [*λ*_{max}, nm (ε, M⁻¹ cm⁻¹): (in MeOH) 715 (80), 610 (sh, 60), 305 (sh, 2300), 267 (7650), 258 (8120), 220 (17 630).

[Cu(L^{NO₂})(OAc)]·MeOH (IV·MeOH)

Yield: 0.52 g (70%). Color: green. Anal. Calcd for C₂₃H₂₄CuN₄O₇: C 51.93, H 4.55, N 10.53. Found: C 51.82, H 4.65, N 10.26. HRMS-ESI(+) (in MeOH with a trace quantity of HCOOH): *m/z* 431.0577 (calculated for C₁₉H₂₀CuN₄O₄ {[Cu(L^{NO₂})]⁺ + 2H₂O - CO₂ - H}⁺: *m/z* 431.0781); 463.0817 (calculated for C₂₀H₁₇CuN₄NaO₄ {[Cu(L^{NO₂})]⁺ + Na⁺ + e⁻}⁺: *m/z* 463.0444). ATR-FTIR (cm⁻¹, solid sample, few selected bands): 3363 (br), 3256 (br), 1567 (s), 1519 (s), 1477 (w), 1408 (s), 1343 (s). UV-vis [*λ*_{max}, nm (ε, M⁻¹ cm⁻¹): (in MeOH) 718 (70), 610 (sh, 60), 264 (13 380), 205 (20 610).

Synthesis of copper(II)-flavonolate adducts [Cu(L^R)(fla)]

A mixture of 3-hydroxyflavone (flaH) (0.23 g, 0.97 mmol) and Me₄NOH·5H₂O (0.18 g, 0.97 mmol) in methanol (10 mL) was

added dropwise to a methanol (10 mL) solution of [Cu(L^R)(OAc)] (0.97 mmol) at room temperature. The mixture was magnetically stirred for 6 hours under a dinitrogen atmosphere. After filtration the addition of diethylether to the filtrate initiated the precipitation of the solid products. The resulting copper(II)-flavonolate adducts were isolated as a green powder by filtration. The pure products were obtained by slow diffusion of hexane into the CH₂Cl₂ solutions of the complexes. Single crystals for the X-ray diffraction of complexes **1** and **2** were also obtained by this method. The yields and other characterization data of all four adducts are given below.

[Cu(L^{OMe})(fla)]·CH₂Cl₂·1.5H₂O (1·CH₂Cl₂·1.5H₂O)

Yield: 0.48 g (~64%). Anal. Calcd for C₃₇H₃₄Cl₂CuN₃O_{7.5}: C 57.33, H 4.42, N 5.42. Found: C 57.22, H 4.35, N 5.56. HRMS-ESI(+) (in MeOH): *m/z* 381.0892 (calculated for C₂₀H₂₀CuN₃O₅ {[Cu(L^{OMe})(fla)] - fla - CO₂}⁺: *m/z* 381.0902); 663.1425 (calculated for C₃₆H₃₀CuN₃O₆ {[Cu(L^{OMe})(fla)] + H⁺}⁺: *m/z* 663.1431). ATR-FTIR (cm⁻¹, solid sample, selected bands): 3378 (br), 3255 (br) (ν(O-H) stretch of solvated water); 1608 (s), 1594 (s) (ν_{asym}(COO)); 1571 (m) (ν(C=O) stretch of coordinated flavonolate); 1440 (m) (ν_{sym}(COO)). UV-vis [*λ*_{max}, nm (ε, M⁻¹ cm⁻¹): (in MeOH) 672 (75), 408 (9800), 330 (sh, 8700), 252 (37 470).

[Cu(L^H)(fla)]·CH₂Cl₂·H₂O (2·CH₂Cl₂·H₂O)

Yield: 0.45 g (63%). Anal. Calcd for C₃₆H₃₁Cl₂CuN₃O₆: C 58.74, H 4.24, N 5.71. Found: C 58.62, H 4.12, N 5.62. HRMS-ESI(+) (in MeOH): *m/z* 351.0824 (calculated for C₁₉H₁₈CuN₃ {[Cu(L^H)(fla)] - fla - CO₂}⁺: *m/z* 351.0797); 633.1346 (calculated for C₃₅H₂₈CuN₃O₅ {[Cu(L^H)(fla)] + H⁺}⁺: *m/z* 633.1325). ATR-FTIR (cm⁻¹, solid sample, selected bands): 3430 (br), 3250 (br) (ν(O-H) stretch of solvated water); 1626 (m), 1615 (m), 1593 (s) (ν_{asym}(COO)); 1573 (m) (ν(C=O) stretch of coordinated flavonolate); 1441 (m) (ν_{sym}(COO)). UV-vis [*λ*_{max}, nm (ε, M⁻¹ cm⁻¹): (in MeOH) 676 (52), 413 (9530), 330 (sh, 5950), 254 (23 710).

[Cu(L^{Cl})(fla)]·2H₂O (3·2H₂O)

Yield: 0.52 g (76%). Anal. Calcd for C₃₅H₃₀ClCuN₃O₇: C 59.74, H 4.30, N 5.97. Found: C 59.62, H 4.25, N 5.86. HRMS-ESI(+) (in MeOH): *m/z* 385.0468 (calculated for C₁₉H₁₇ClCuN₃ {[Cu(L^{Cl})(fla)] - fla - CO₂}⁺: *m/z* 385.0407); 667.1025 (calculated for C₃₅H₂₇ClCuN₃O₅ {[Cu(L^{Cl})(fla)] + H⁺}⁺: *m/z* 667.0935). ATR-FTIR (cm⁻¹, solid sample, selected bands): 3400 (br), 3270 (br) (ν(O-H) stretch of solvated water); 1607 (s), 1595 (s) (ν_{asym}(COO)); 1574 (m) (ν(C=O) stretch of coordinated flavonolate); 1488 (m), 1444 (m) (ν_{sym}(COO)). UV-vis [*λ*_{max}, nm (ε, M⁻¹ cm⁻¹): (in MeOH) 676 (35), 420 (9280), 330 (sh, 5340), 254 (20 870).

[Cu(L^{NO₂})(fla)]·3H₂O (4·3H₂O)

Yield: 0.46 g (65%). Anal. Calcd for C₃₅H₃₂CuN₄O₁₀: C 57.41, H 4.41, N 7.65. Found: C 57.37, H 4.55, N 7.72. HRMS-ESI(+) (in MeOH): *m/z* 678.2004 (calculated for C₃₅H₂₇CuN₄O₇ {[Cu(L^{NO₂})(fla)] + H⁺}⁺: *m/z* 678.1176). ATR-FTIR (cm⁻¹, solid sample,

selected bands): 3345 (br), 3250 (br) ($\nu(\text{O-H})$ stretch of solvated water); 1587 (sh) ($\nu(\text{C=O})$ stretch of coordinated flavonolate); 1563 (s) ($\nu_{\text{asym}}(\text{COO})$), 1518 (s) ($\nu_{\text{asym}}(\text{NO}_2)$); 1487 (m) ($\nu_{\text{sym}}(\text{COO})$), 1342 (s) ($\nu_{\text{sym}}(\text{NO}_2)$). UV-vis [λ_{max} , nm (ϵ , $\text{M}^{-1} \text{cm}^{-1}$): (in MeOH) 650 (50), 421 (8980), 330 (sh, 5850), 256 (24 420).

Synthesis of $[\text{Zn}(\text{L}^{\text{OMe}})(\text{fla})]\cdot 2\text{H}_2\text{O}$ (**5**· $2\text{H}_2\text{O}$)

To a magnetically stirred solution of ligand LiL^{OMe} (0.063 g, 0.17 mmol) in methanol (10 mL), a methanolic solution (5 mL) of $\text{Zn}(\text{OAc})_2\cdot 2\text{H}_2\text{O}$ (0.037 g, 0.17 mmol) was added dropwise, resulting in a pale yellow solution. After 1 hour of stirring at room temperature a mixture of 3-hydroxyflavone (0.041 g, 0.17 mmol) and $\text{Me}_4\text{NOH}\cdot 5\text{H}_2\text{O}$ (0.031 g, 0.17 mmol) in methanol (5 mL) was added dropwise under anaerobic conditions. The resulting yellow reaction mixture was magnetically stirred for 6 hours at room temperature in a dinitrogen atmosphere. It was then filtered and the addition of diethylether to the filtrate initiated the precipitation of the products as a pale-yellow solid. Slow diffusion of diethylether into the methanolic solution of the product yielded the complex as a micro-crystalline yellow solid. Single crystals obtained from this method were found to be suitable for structural analysis by X-ray diffraction. Yield: 0.087 g (75%). Anal. Calcd for $\text{C}_{36}\text{H}_{33}\text{N}_3\text{O}_8\text{Zn}$: C 61.68, H 4.74, N 5.99. Found: C 61.62, H 4.68, N 6.06. HRMS-ESI(+) (in MeOH): m/z 426.0809 (calculated for $\text{C}_{21}\text{H}_{20}\text{N}_3\text{O}_3\text{Zn} \{[\text{Zn}(\text{L}^{\text{OMe}})(\text{fla})] - \text{fla}\}^+$; m/z 426.0796); 664.1423 (calculated for $\text{C}_{36}\text{H}_{30}\text{N}_3\text{O}_6\text{Zn} \{[\text{Zn}(\text{L}^{\text{OMe}})(\text{fla})] + \text{H}^+\}^+$; m/z 664.1426). ATR-FTIR (cm^{-1} , solid sample, selected bands): 3350 (br), 3265 (br) ($\nu(\text{O-H})$ stretch of solvated water); 1569 (s) ($\nu_{\text{asym}}(\text{COO})$); 1556 ($\nu(\text{C=O})$ stretch of coordinated flavonolate); 1408 (s) ($\nu_{\text{sym}}(\text{COO})$). UV-vis [λ_{max} , nm (ϵ , $\text{M}^{-1} \text{cm}^{-1}$): (in MeOH) 409 (9100), 320 (sh, 3460), 251 (16 445), 229 (18 170). ^1H NMR (500 MHz, 300 K, CD_3OD): δ (ppm) = 8.92 (br, 1H), 8.61 (d, 2H, $J = 10$ Hz), 8.22 (d, 2H, $J = 10$ Hz), 7.90 (t, 2H, $J = 5$ Hz), 7.72 (d, 1H, $J = 10$ Hz), 7.67–7.69 (m, 2H), 7.63 (d, 1H, $J = 10$ Hz), 7.50 (t, 1H, $J = 5$ Hz), 7.43 (t, 2H, $J = 5$ Hz), 7.35–7.38 (m, 3H), 7.30 (t, 2H, $J = 5$ Hz), 6.86 (d, 2H, $J = 10$ Hz), 5.41 (s, 1H, $\text{Py}_2\text{CHN-}$), 3.94 (d, 1H, $J_{\text{cd}} = 15$ Hz, $-\text{NCH}^{\text{c}}\text{H}^{\text{d}}\text{Ph}$), 3.74 (d, 1H, $J_{\text{cd}} = 15$ Hz, $-\text{NCH}^{\text{c}}\text{H}^{\text{d}}\text{Ph}$), 3.70 (s, 3H, $-\text{OCH}_3$), 3.42 (d, 1H, $J_{\text{ab}} = 15$ Hz, $-\text{NCH}^{\text{a}}\text{H}^{\text{b}}\text{COO}$), 2.69 (d, 1H, $J_{\text{ab}} = 15$ Hz, $-\text{NCH}^{\text{a}}\text{H}^{\text{b}}\text{COO}$). ^{13}C NMR (125 MHz, 300 K, CD_3OD): δ (ppm) = 192.32, 178.94, 160.00, 155.36, 154.72, 149.34, 149.18, 140.31, 140.16, 133.66, 132.60, 132.10, 128.40, 127.92, 127.12, 125.37, 124.96, 124.89, 124.74, 124.27, 123.74, 119.47, 118.02, 113.81, 69.23 ($\text{Py}_2\text{CHN-}$), 55.59 ($-\text{NCH}_2\text{Ph}$), 54.52 ($-\text{OCH}_3$), 51.94 ($-\text{NCH}_2\text{COO}$).

General instrumentation

The following instruments were used for various spectroscopic measurements: (i) an Agilent 8454 diode-array spectrophotometer for UV-vis spectroscopy; (ii) a PerkinElmer spectrum two FT-IR spectrometer (range 4000–400 cm^{-1}) for the attenuated-total-reflectance Fourier transform infrared (ATR-FTIR) spectroscopy; (iii) an Agilent 6545XT AdvanceBio LC/Q-TOF spectrometer or Waters Xevo G2 QToF spectrometer for HRMS-ESI(+);

(iv) a Bruker 400/500 Ultrashield (400 MHz/500 MHz) NMR spectrometer for NMR; chemical shifts are reported in ppm with reference to the solvent residual peak; (v) a Bruker ELEXSYS 580 spectrometer for X-band EPR spectroscopy. Elemental analyses (C, H, N) were carried out using a PerkinElmer Elemental Analyzer (Model No 2400SERIESII). Product analyses by GC-MS were performed on a Thermo Scientific Trace 1300 gas chromatograph connected to an ISQ single quadrupole MS. Cyclic voltammograms were recorded by using the CH Instruments Electrochemical Analyzer/Workstation Model 660E Series. A standard three-electrode cell with a glassy carbon working electrode (diameter: 3 mm), a platinum-wire auxiliary electrode, and a saturated calomel electrode (SCE) as the reference was employed to perform the electrochemical measurements.

X-ray crystallography

Single crystal X-ray diffraction data of complexes **I**· $2\text{H}_2\text{O}$, **II**·MeOH, **III**· $2\text{H}_2\text{O}$, **IV**·MeOH, **1**· $\text{CH}_2\text{Cl}_2\cdot 1.5\text{H}_2\text{O}$, **2**· $\text{CH}_2\text{Cl}_2\cdot \text{H}_2\text{O}$ and **5**· $2\text{H}_2\text{O}$ were collected on a Bruker SMART APEXII CCD diffractometer with graphite-monochromated Mo-K α ($\lambda = 0.71073 \text{ \AA}$) radiation. All data were collected at 296 K. The “Bruker Saint Plus” program was used for data reduction. The corrections of data for Lorentz and polarization effects were performed. An empirical absorption correction (SADABS 2016/2) was applied. The structures were solved by SIR-2014 and refined by full-matrix least squares methods based on F^2 using SHELXL-2018/3, incorporated in a WinGX 2021.2 crystallographic collective package.²¹ All non-hydrogen atoms of the seven complexes were refined anisotropically. In the case of **II**·MeOH, the asymmetric unit contains two molecules. For **I**· $2\text{H}_2\text{O}$ and **III**· $2\text{H}_2\text{O}$ some disorders were encountered with the oxygen atom of one of the water molecules. The disorder of the respective oxygen atom was fixed with a site occupation factor of 80/20 (for **I**· $2\text{H}_2\text{O}$) and 57/43 (for **III**· $2\text{H}_2\text{O}$). For **I**· $2\text{H}_2\text{O}$ the positions of the hydrogen atoms of the O1W-labelled water molecule were located from the difference Fourier map; however, for the disordered solvent water molecule the hydrogen atoms could not be assigned. Also we could not locate the hydrogen atoms of the solvent molecules (water or methanolic OH) for other six complexes as well. Thus, the refinement of such oxygen atoms of the solvent molecules was performed without hydrogen atoms linked to them, but they are added to the formula. Other than that, the positions of all hydrogen atoms were calculated assuming ideal geometries for all complexes. For **1**· $\text{CH}_2\text{Cl}_2\cdot 1.5\text{H}_2\text{O}$ two residual Q-peaks at 1.16 e\AA^{-3} and 1.12 e\AA^{-3} could not be modelled due to the poor dataset. For **2**· $\text{CH}_2\text{Cl}_2\cdot \text{H}_2\text{O}$ two aromatic carbon atoms C10 and C11 were refined with equal thermal parameters using the EADP command. The crystal quality of **5**· $2\text{H}_2\text{O}$ was poor, but still data were collected with such a crystal as this was the best we could obtain. In **5**· $2\text{H}_2\text{O}$ a few atoms showed large displacement parameters, which was probably due to the poor quality of the data. Pertinent crystallographic parameters of the four acetate bound complexes **I**· $2\text{H}_2\text{O}$ (CCDC 2112719), **II**·MeOH (CCDC 2112720), **III**· $2\text{H}_2\text{O}$ (CCDC 2112721), and **IV**·MeOH

(CCDC 2112723), and the three flavonolate adducts **1**·CH₂Cl₂·1.5H₂O (CCDC 2112724), **2**·CH₂Cl₂·H₂O (CCDC 2112725) and **5**·2H₂O (CCDC 2112726) are presented in Tables S1 and S2 (ESI),[†] respectively. The torsion and dihedral angles were measured using the Diamond 4 programme.

Reaction product analysis

By GC-MS. The oxygenative degradation of the ES model complexes ($[1-5] = 1 \times 10^{-2}$ M) was carried out in DMF at 80 °C under a continuous flow of dioxygen for about 10–14 hours. After that solvent DMF was removed completely from each reaction solution. The organic substances were extracted with a 1 : 1 mixture of CH₂Cl₂ and diethylether. Evaporation of the solvent yielded a yellowish white residue which was subjected to GC-MS analysis using methanol as an eluent and helium as a carrier gas.

By ¹H NMR. The product analysis with complex [Cu(L^H)(fla)] (**2**) was also carried out by ¹H NMR spectroscopy. In a typical experiment, 1×10^{-2} M solution of the complex in DMF was heated at 80 °C under a continuous flow of dioxygen for 5 h. After removal of the solvent, the residue was treated with a 1 : 1 mixture of CH₂Cl₂ and diethylether. The organic solvent extract was washed with water. Evaporation of the organic solvent yielded a yellowish white residue which was analysed by ¹H NMR. The spectrum consisted of signals of two main products benzoic acid and salicylic acid, which were identified by comparing their ¹H NMR signal patterns to those of the authentic samples.

Kinetic measurements. The kinetic experiments of the dioxygenation of all enzyme–substrate adducts (complexes **1–5**) at a single-turnover were carried out in DMF at 80 °C in the presence of dioxygen. The progress of each reaction was followed by using a UV-visible spectrophotometer by monitoring the absorbance change of the band due to the $\pi \rightarrow \pi^*$ transition of the coordinated flavonolate. In a typical experiment, 50 mL of 1×10^{-4} M solution of each flavonolate adduct in DMF was taken in a 100 mL two-necked round bottom flask. A water-jacketed condenser was connected to one neck, and the other neck was sealed with a rubber septum. At the start of the experiment, nitrogen gas was bubbled into each solution and the temperature was maintained at 80 °C by immersing the flask into a silicone oil bath. The dioxygenation reaction was initiated by replacing nitrogen with an oxygen gas flow. The oxygen bubbling was continued until the end of the experiment. In each case, 2.5 mL solution of the sample was taken out from the flask at every 5 minutes of time interval and placed in a previously cooled vessel under a nitrogen atmosphere to prevent further degradation of the adduct. The absorbance values of the respective $\pi \rightarrow \pi^*$ band of all sample solutions at various time intervals were measured spectrophotometrically to obtain a time course of degradation of the corresponding adduct.

Computational methods. All calculations were performed using the Orca 4.2.1^{22a} suite of programs. Full geometry optimizations were carried out for all complexes using range separated hybrid density functional ω B97XD3^{22b} in combination with the def2-SVP^{22c} basis set for all atoms. The def2-

ECP pseudopotentials were used for the Cu atom. The RIJCOSX approximation^{22d} with corresponding auxiliary basis sets was used to speed up the calculations. Increased integration grids (Grid6, finalgrid7 in ORCA convention) and tight SCF convergence criteria were used. To ensure that the resulting structures converged to a local minimum on the potential energy surface vibrational frequency calculations were performed which resulted in only positive normal vibrations. Single point energy calculations were then performed with the larger def2-TZVP^{22c} basis set on the ω B97XD/def2-SVP optimized geometries. Solvent effects were accounted for according to the experimental conditions. Hence, we used the DMF solvent ($\epsilon = 38.3$) within the framework of the conductor-like screening (COSMO) dielectric continuum approach.^{22e} The relative energies were computed from the gas phase optimized structures as a sum of electronic energy from def2-TZVP calculations, free energy, and solvent corrections at the def2-SVP level. The transition states were located using the Climbing Image Nudged Elastic Band (CI-NEB) method. The converged geometry from CI was then reoptimized with the transition state optimizer and then characterized with the vibrational frequency analysis to confirm the single imaginary frequency and intrinsic reaction coordinate (IRC) analysis^{22f} to confirm the connection to the correct reactant and products. The minimum energy crossing point (MECP) was optimized using the surface crossing optimization algorithm implemented in ORCA. Mulliken spin population analyses were also carried out to check the spin state values for Cu, O₂, flavonolate, and the rest of the ligand moieties.

Results and discussion

Syntheses, characterization and crystal structures

To mimic the coordination environment of the active site of the 2,4-QD enzyme (*minor* form) we have designed four tetradentate ligand frameworks, L^R (R = -OMe, -H, -Cl, and -NO₂) comprising three N-coordinating sites, corresponding to the three Histidine N-atoms, and one O donor carboxylate group, corresponding to Glu-73. The electronic properties of the ligands are finely tuned by varying the R substituents from electron donating to electron withdrawing at the *para*-position of the benzyl group. The ligands were synthesized by a multi-step procedure and were isolated as lithium salts, LiL^R. The synthetic protocols are shown in Schemes S1 and S2 in the ESI.[†] All four ligands were characterized by various spectroscopic [HRMS-ESI(+), IR and ¹H NMR] techniques (see the Experimental section and Fig. S1–S9 in the ESI[†]). The treatment of the ligands with Cu(OAc)₂·H₂O in a 1 : 1 molar ratio in methanol yielded the corresponding acetate bound mononuclear copper(II) complexes, [Cu^{II}(L^R)(OAc)] (**I–IV**). The purity of the complexes was authenticated by elemental analyses. All four complexes were characterized by HRMS-ESI(+), IR, and UV-vis spectroscopy (see the Experimental section and Fig. S10–S15 in the ESI[†]). In the UV-vis spectra of complexes **I–IV**, we observed an order of -OMe (**I**) < -H (**II**) < -Cl(**III**) < -NO₂

(IV) for the λ_{\max} values of the $d-d$ band (Fig. S16[†]), implying that the substituent groups influence the relative energy gap of the $d-d$ transitions. The structural analyses of compounds **I**·2H₂O, **II**·MeOH, **III**·2H₂O and **IV**·MeOH were performed by single crystal X-ray diffraction. The ORTEP drawing of the four complexes is shown in Fig. 2. Selected bond lengths and bond angles are summarized in Tables S3–S6.[†] Structural analysis reveals that the Cu(II) ion in each complex exhibits a distorted square-pyramidal geometry [τ values 0.25 (**I**·2H₂O), 0.17 (**II**·MeOH, average value), 0.26 (**III**·2H₂O), and 0.26 (**IV**·MeOH)]²³ with an N₃O₂ donor set. In the respective complex the three equatorial positions are occupied by three donor sites of the tetradentate ligand *via* a *tert*-alkylamine nitrogen atom, one of the pyridine nitrogen atoms, and the carboxylate oxygen atom; whereas the axial position is occupied by the other pyridine nitrogen atom. The fourth equatorial position in each complex is occupied by the carboxylate oxygen atom of the acetate co-ligand. Due to the Jahn–Teller effect the axial Cu–N(pyridine) bond in each complex is elongated as compared to the equatorial bonds. The bond angles around the Cu(II) centre deviate from the ideal square-pyramidal angles in the four complexes, implying a distortion from the ideal geometry (Tables S3–S6[†]).

The reaction of [Cu(L^R)(OAc)] with 3-hydroxyflavone (flaH) and Me₄NOH·5H₂O in methanol under inert conditions gave the corresponding copper(II)-flavonolate adducts **1–4**. The formation of 1 : 1 [Cu(L^R)(fla)] adducts was confirmed by spectroscopic titrations (Fig. S17[†]). Upon addition of flaH in the presence of a base to a methanol solution of the corresponding [Cu(L^R)(OAc)] complex under inert conditions at room temperature, an intense band in the range of 408–421 nm due to $\pi \rightarrow \pi^*$ transition for the coordinated flavonolate was observed.^{11,24} The intensities of the $\pi \rightarrow \pi^*$ band in each case increased steadily with incremental addition of fla[−] up to one equivalent, which then reached a plateau upon further addition of the fla[−] ion. From the spectrophotometric titration (see the ESI[†] for details) the equilibrium constant (K_{eq}) values

are determined to be 12.35 ± 0.78 (**1**), 15.08 ± 1.54 (**2**), 14.42 ± 0.93 (**3**) and 16.13 ± 0.78 (**4**) (Fig. S18[†]). The higher values of the equilibrium constants confirmed the facile formation of the 1 : 1 Cu-flavonolate adducts [Cu(L^R)(fla)] in solution. Due to the higher stability of the copper-flavonolate adducts at room temperature we could isolate them as a solid in a moderately good yield. Pure products of chemical formulas [Cu(L^{OMe})(fla)]·CH₂Cl₂·1.5H₂O (**1**·CH₂Cl₂·1.5H₂O), [Cu(L^H)(fla)]·CH₂Cl₂·H₂O (**2**·CH₂Cl₂·H₂O), [Cu(L^{Cl})(fla)]·2H₂O (**3**·2H₂O) and [Cu(L^{NO₂})(fla)]·3H₂O (**4**·3H₂O) were obtained by recrystallization from CH₂Cl₂/hexane. All complexes were characterized by elemental analyses and by using various spectroscopic techniques. Structural analyses of **1**·CH₂Cl₂·1.5H₂O and **2**·CH₂Cl₂·H₂O were performed by X-ray diffraction.

The IR spectra of complexes **1–4** are shown in Fig. S19.[†] In each spectrum a moderately strong band at 1571 cm^{−1} (**1**), 1573 cm^{−1} (**2**), 1574 cm^{−1} (**3**) and 1587 (sh) cm^{−1} (**4**) due to the $\nu(\text{C}=\text{O})$ stretching vibration of the coordinated carbonyl group of fla[−] is observed. In all cases the bands are red shifted as compared with those of the free flavonol (1602 cm^{−1}). Such a lowering was also found with other coordinated flavonolate complexes.^{6,13,17–19} The characteristic $\nu_{\text{asym}}(\text{COO})$ and $\nu_{\text{sym}}(\text{COO})$ bands of the carboxylate groups of L^R in all Cu(II) ES adducts appear in the ranges of 1563–1626 cm^{−1} and 1440–1488 cm^{−1}, respectively. The small difference between the two vibrations (<200 cm^{−1}) suggests a monodentate carboxylate binding mode in all adducts (*vide infra*).²⁵ In all spectra a broad band in the range of 3250–3430 cm^{−1} has also been observed. This may be assigned to the $\nu(\text{OH})$ stretching vibration of the solvated water molecules present in each complex as the solvent of crystallization. In the HRMS-ESI(+) spectra, detection of the molecular ion peak corresponding to species {[Cu(L^R)(fla)] + H⁺}⁺ confirms the formation of the 1 : 1 adduct in all cases (Fig. S20–S23[†]). The observed m/z value of the respective species agrees well with the calculated value (see the Experimental section). The electronic spectra of the copper(II)-flavonolate complexes are shown in Fig. S24[†] and consist of

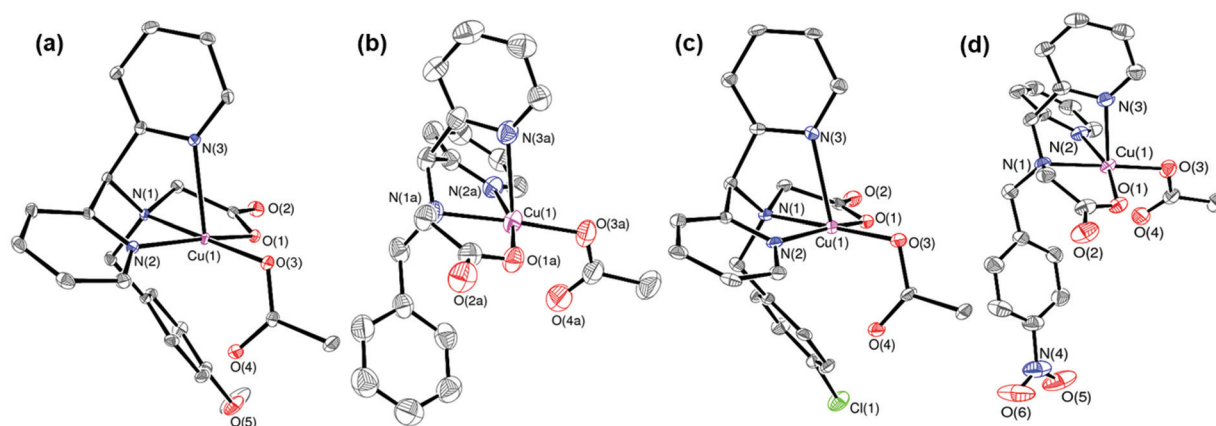


Fig. 2 ORTEP (30% ellipsoid) diagram of complexes (a) [Cu(L^{OMe})(OAc)]·2H₂O (**I**·2H₂O), (b) [Cu(L^H)(OAc)]·MeOH (**II**·MeOH), (c) [Cu(L^{Cl})(OAc)]·2H₂O (**III**·2H₂O), and (d) [Cu(L^{NO₂})(OAc)]·MeOH (**IV**·MeOH). Carbon atoms are not labelled. The hydrogen atoms are omitted for clarity. The solvent molecules are not shown for clarity.

several absorption bands. The methanol solutions of the complexes exhibit a low intense band in the visible region at 672 nm ($\epsilon = 75 \text{ M}^{-1} \text{ cm}^{-1}$) for **1**, 676 nm ($\epsilon = 52 \text{ M}^{-1} \text{ cm}^{-1}$) for **2**, 676 nm ($\epsilon = 35 \text{ M}^{-1} \text{ cm}^{-1}$) for **3**, and 650 nm ($\epsilon = 50 \text{ M}^{-1} \text{ cm}^{-1}$) for **4**, which can be assigned to $d-d$ transitions.²⁶ For all complexes, several high intensity charge transfer bands dominate the lower wavelength region. The $\pi \rightarrow \pi^*$ transition due to the coordinated flavonolate appears at 408 nm ($\epsilon = 9800 \text{ M}^{-1} \text{ cm}^{-1}$) for **1**, 413 nm ($\epsilon = 9530 \text{ M}^{-1} \text{ cm}^{-1}$) for **2**, 420 nm ($\epsilon = 9280 \text{ M}^{-1} \text{ cm}^{-1}$) for **3**, and 421 nm ($\epsilon = 8980 \text{ M}^{-1} \text{ cm}^{-1}$) for **4**. It has to be noted that this band is blue-shifted relative to that of Kfla (465 nm)^{24b} for each complex. Besides that, several other intra-ligand charge transfer bands are observed in the range of 252–330 nm for all complexes. The plot of λ_{max} of the $\pi \rightarrow \pi^*$ transition of coordinated fl⁻ versus the Hammett constants (σ) of the substituent groups in complexes **1–4** is shown in Fig. S25.† Notably, the Hammett constants (σ) of the substituent groups –OMe (**1**), –H (**2**) and –Cl (**3**) are linearly correlated ($R = 0.99$) with λ_{max} of fl⁻; whereas the –NO₂ (**4**) group

deviates from the linear relationship.^{27a} This might be due to the larger impact on the solvation free energy, transition dipole moment, and static dipole differences of the electron withdrawing groups than that on the electron donating groups,^{27b} which might influence the energy levels of the orbitals. Thus, it is apparent that the relative energy differences in the $\pi \rightarrow \pi^*$ transitions of fl⁻ in complexes **1–4** are perturbed by the electronic nature of the substituent groups in the ligands *via* the Cu(II) centre. The EPR spectra of all four complexes were recorded in methanol at 298 K. The experimental and the simulated spectra are displayed in Fig. S26.† The EPR spectra were simulated using the EasySpin software package (version 5.2.32).²⁸ Complexes **1** and **2** show an isotropic signal ($g_{\text{iso}} > 2$) with hyperfine interaction with the Cu-nucleus; whereas complexes **3** and **4** show an axial type signal ($g_{\parallel} > g_{\perp} > 2$) where hyperfine splitting was observed with the g_{\perp} signal. All spectra could be simulated considering $S = \frac{1}{2}$ spin using the g - and A -values given in Table S7,† attesting to the mononuclear structure of the ES adducts in the solution phase. In all cases anisotropic line broadening due to g -strain and A -strain was needed to obtain a good simulation, probably reflecting the distorted octahedral geometry around the Cu(II) ions.

The structural analyses of **1**·CH₂Cl₂·1.5H₂O and **2**·CH₂Cl₂·H₂O confirm the formation of the 1 : 1 ES adduct as shown in Fig. 3. The selected bond lengths and bond angles are tabulated in Table 1. The Cu(II) centre of each ES adduct adopts a tetragonally elongated octahedral geometry with a N₃O₃ donor set consisting of two oxygen atoms of flavonolate (O(3): 3-hydroxylate and O(4): 4-carbonyl), one oxygen atom O(1) of the carboxylate of L^R, and three nitrogen atoms (one *tert*-amine nitrogen N(1) and two pyridyl nitrogen donors N(2) & N(3)) of ligand L^R. The carbonyl O(4) atom of fl⁻ and the

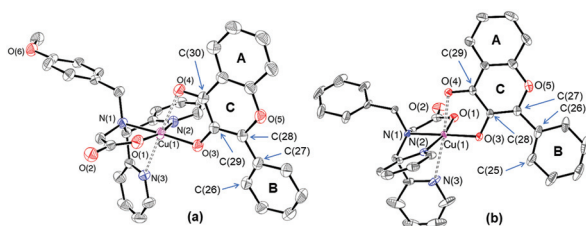


Fig. 3 ORTEP (30% ellipsoid) diagram of complexes (a) [Cu(L^{OMe})(fla)]·CH₂Cl₂·1.5H₂O (**1**·CH₂Cl₂·1.5H₂O), and (b) [Cu(L^H)(fla)]·CH₂Cl₂·H₂O (**2**·CH₂Cl₂·H₂O). Hydrogen atoms and solvent molecules are omitted for clarity.

Table 1 Selected bond lengths (Å) and bond angles (°) of **1**·CH₂Cl₂·1.5H₂O, **2**·CH₂Cl₂·H₂O and **5**·2H₂O

1 ·CH ₂ Cl ₂ ·1.5H ₂ O		2 ·CH ₂ Cl ₂ ·H ₂ O		5 ·2H ₂ O	
Cu(1)–N(1)	2.054(2)	Cu(1)–N(1)	2.039(3)	Zn(1)–N(1)	2.317(5)
Cu(1)–N(2)	2.034(3)	Cu(1)–N(2)	2.005(4)	Zn(1)–N(2)	2.194(6)
Cu(1)–N(3)	2.527(4)	Cu(1)–N(3)	2.619(4)	Zn(1)–N(3)	2.217(5)
Cu(1)–O(1)	1.953(2)	Cu(1)–O(1)	1.954(3)	Zn(1)–O(1)	2.019(5)
Cu(1)–O(3)	1.917(2)	Cu(1)–O(3)	1.936(3)	Zn(1)–O(3)	2.019(5)
Cu(1)–O(4)	2.411(3)	Cu(1)–O(4)	2.367(3)	Zn(1)–O(4)	2.149(5)
C(29)–O(3)	1.308(4)	C(28)–O(3)	1.317(5)	C(29)–O(3)	1.378(8)
C(30)–O(4)	1.242(4)	C(29)–O(4)	1.232(5)	C(30)–O(4)	1.219(8)
N(1)–Cu(1)–N(2)	81.48(10)	N(1)–Cu(1)–N(2)	81.37(14)	N(1)–Zn(1)–N(2)	73.62(19)
N(1)–Cu(1)–N(3)	73.16(10)	N(1)–Cu(1)–N(3)	73.32(13)	N(1)–Zn(1)–N(3)	75.10(18)
N(2)–Cu(1)–N(3)	80.94(10)	N(2)–Cu(1)–N(3)	77.60(14)	N(2)–Zn(1)–N(3)	83.4(2)
N(1)–Cu(1)–O(1)	83.63(9)	N(1)–Cu(1)–O(1)	84.20(14)	N(1)–Zn(1)–O(1)	77.7(2)
N(1)–Cu(1)–O(3)	174.51(9)	N(1)–Cu(1)–O(3)	178.85(13)	N(1)–Zn(1)–O(3)	123.6(2)
N(1)–Cu(1)–O(4)	107.68(8)	N(1)–Cu(1)–O(4)	103.79(12)	N(1)–Zn(1)–O(4)	156.16(19)
N(2)–Cu(1)–O(1)	165.04(10)	N(2)–Cu(1)–O(1)	165.54(13)	N(2)–Zn(1)–O(1)	150.2(2)
N(2)–Cu(1)–O(3)	94.89(11)	N(2)–Cu(1)–O(3)	97.83(14)	N(2)–Zn(1)–O(3)	90.1(2)
N(2)–Cu(1)–O(4)	94.85(10)	N(2)–Cu(1)–O(4)	95.04(12)	N(2)–Zn(1)–O(4)	111.8(2)
N(3)–Cu(1)–O(1)	96.11(11)	N(3)–Cu(1)–O(1)	98.98(13)	N(3)–Zn(1)–O(1)	97.1(2)
N(3)–Cu(1)–O(3)	102.27(10)	N(3)–Cu(1)–O(3)	105.72(12)	N(3)–Zn(1)–O(3)	157.6(2)
N(3)–Cu(1)–O(4)	175.58(11)	N(3)–Cu(1)–O(4)	172.36(10)	N(3)–Zn(1)–O(4)	82.4(2)
O(1)–Cu(1)–O(3)	100.06(10)	O(1)–Cu(1)–O(3)	96.61(13)	O(1)–Zn(1)–O(3)	99.0(2)
O(1)–Cu(1)–O(4)	88.30(10)	O(1)–Cu(1)–O(4)	87.63(12)	O(1)–Zn(1)–O(4)	97.7(2)
O(3)–Cu(1)–O(4)	76.63(8)	O(3)–Cu(1)–O(4)	77.08(11)	O(3)–Zn(1)–O(4)	80.1(2)

N(3) atom of the pyridyl group of the ligand occupy the axial positions in both structures. The Cu–O_{carboxylate} bond length of both complexes [1.953(2) Å for **1**·CH₂Cl₂·1.5H₂O and 1.954(2) Å for **2**·CH₂Cl₂·H₂O] is much shorter than that of the Cu–O_{Glu73} distance (2.28 Å) of the natural ES adduct of 2,4-QD.³ Thus in the present model complexes the carboxylate oxygen binds relatively strongly to the Cu(II) centre, as a consequence of the formation of a stable five-membered ring. The axial Cu–O_{4-carbonyl} and Cu–N_{pyridyl} bond distances are relatively long compared to the equatorial bond distances in both adducts (see Table 1). Such an elongation is a result of Jahn–Teller distortion expected for the *d*⁹ Cu(II) system. The Cu–(fla)O_{4-carbonyl} and Cu–(fla)O_{3-hydroxylate} bond lengths are 2.411(3) & 1.917(2) Å for **1**·CH₂Cl₂·1.5H₂O, and 2.367(3) & 1.936(3) Å for **2**·CH₂Cl₂·H₂O, respectively. In natural 2,4-QD, the distance of Cu–(fla)O_{3-hydroxyl} is 2.29 Å, whereas the carbonyl O4 of flavonol resides at a non-coordinating distance of about 3.5 Å from the copper centre, interpreting a monodentate mode of binding of flavonol in the enzymatic system.³ The differences between the two distances [$\Delta d(\text{Cu–O}) = d\text{Cu–(fla)O}_{4\text{-carbonyl}} - d\text{Cu–(fla)O}_{3\text{-hydroxylate}}$] for **1**·CH₂Cl₂·1.5H₂O and **2**·CH₂Cl₂·H₂O are 0.494 Å and 0.431 Å, respectively, which are shorter than those of natural 2,4-QD (1.21 Å). However, it has to be noted here that these $\Delta d(\text{Cu–O})$ values of the present ES adducts are much higher than those of all of the reported Cu^{II}-flavonolate ES model complexes (0.043–0.264 Å).⁸ Thus, it may be attributed to the fact that the substrate flavonolate is inclined to a monodentate mode of binding *via* O(3-hydroxylate) in complexes **1**·CH₂Cl₂·1.5H₂O and **2**·CH₂Cl₂·H₂O with a weak interaction from the carbonyl O(4) of the fla[−] ion. For both complexes, interestingly, the substrate flavonolate bound to the copper(II) centre is bent at the carbon atom C(28) for **1**·CH₂Cl₂·1.5H₂O and C(27) for **2**·CH₂Cl₂·H₂O. The torsion angles measured at C(29)–C(28)–C(27)–C(26) for **1**·CH₂Cl₂·1.5H₂O and at C(28)–C(27)–C(26)–C(25) for **2**·CH₂Cl₂·H₂O are 8.5(5)° and 12.0(7)°, respectively, indicating that the C(28)/C(27) atom of the respective complex (corresponding to C(2) of the enzymatic substrate as shown in Scheme 1) possesses some sp³ character by pyramidalization. This phenomenon was also observed in the ES adduct of 2,4-QD from *Aspergillus japonicus*.³ This is ascribed to the stabilization of a carbon-centered radical activated for the dioxygen attack in the enzymatic reaction. The plane comprising the C-ring atoms and donors O(3) and O(4) of substrate flavonolate is slanted to a certain degree from the coordination plane *viz* O(3)–Cu(1)–O(4) in both complexes. The dihedral angles between them are found to be 4.793(83)° and 15.665(95)° for **1**·CH₂Cl₂·1.5H₂O and **2**·CH₂Cl₂·H₂O, respectively, which may influence the electronic communication between the substrate flavonolate and peripheral ligand *via* the Cu(II) ion. Such a structural and conformation unevenness of the bound substrate flavonolate may be caused by the substituent group in the supporting model ligand, which may lead to the difference in the reactivity of the complexes, as observed below.

In addition to the Cu-flavonolate complexes, we synthesized an additional zinc(II)-flavonolate complex with ligand L^{OMe} to

understand the initial electron transfer process during the dioxygenation of the flavonolate adducts. The complex was synthesized by a one pot reaction of ligand LiL^{OMe} with Zn(OAc)₂·2H₂O, flavonol and Me₄NOH·5H₂O as a base in methanol at room temperature under inert conditions. Recrystallization of the crude product from MeOH/Et₂O afforded analytically pure complex [Zn(L^{OMe})(fla)]·2H₂O (**5**·2H₂O), which was authenticated by elemental analysis. The crystal structure shows that the Zn(II) centre adopts a distorted octahedral geometry, where the substrate flavonolate binds in a bidentate chelating fashion and the remaining four coordination sites are occupied by the supporting L^{OMe} ligand (see Fig. 4 and Table 1). Similar to the Cu(II)-ES adducts described above the phenyl group (B-ring) of the bound flavonolate is bent out from the C-ring plane due to pyramidalization at the C(28) atom. The torsion angle at C(29)–C(28)–C(27)–C(26) is determined to be 8.453(1303)°, which is comparable to that found for the Cu(II)-adducts.

Complex **5**·2H₂O was also characterized by various spectroscopic techniques such as UV-vis, ATR-FTIR, HRMS-ESI(+) and NMR (see the Experimental section). In the UV-vis spectrum, the characteristic $\pi \rightarrow \pi^*$ transition due to the coordinated flavonolate occurs at 409 nm ($\epsilon = 9100 \text{ M}^{-1} \text{ cm}^{-1}$) (Fig. S27†). The ATR-FTIR spectrum (Fig. S28†) of the solid sample shows the carbonyl group stretching vibration $\nu(\text{CO})$ of the coordinated flavonolate at 1556 cm^{−1}, which is lower than those of the Cu-fla complexes. This might be due to the difference in the M–O(4) bond distance (see Table 1), concerning diverse geometrical preferences amongst the Zn(II) and Cu(II) ions. The asymmetric $\nu_{\text{asym}}(\text{COO})$ and symmetric $\nu_{\text{sym}}(\text{COO})$ bands of the carboxylate group of the ligand appear at 1569 cm^{−1} and 1408 cm^{−1}, respectively, attesting to the monodentate binding mode of the carboxylate group ($\Delta\nu < 200 \text{ cm}^{-1}$)²⁵ as found in the X-ray structure. The HRMS-ESI(+) spectrum of the compound (Fig. S29†) in methanol shows a signal at *m/z* = 664.1423 (calc. 664.1426) corresponding to the species { [Zn(L^{OMe})(fla)] + H⁺ }⁺, which confirms the mononuclear structure of the complex in solution. The Zn(II) ion being diamagnetic in nature, complex

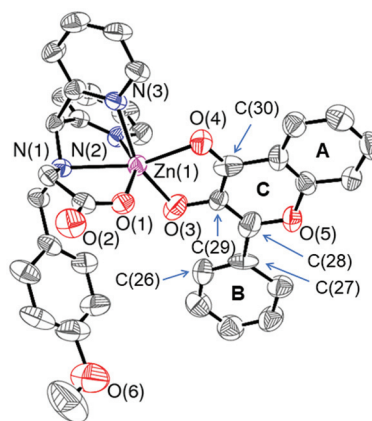


Fig. 4 ORTEP (30% ellipsoid) diagram of complex [Zn(L^{OMe})(fla)]·2H₂O (**5**·2H₂O). Hydrogen atoms and solvent molecules are omitted for clarity.

5·2H₂O was also characterized by 1D and 2D NMR spectroscopy (Fig. S30–S32†). The ¹H NMR spectrum of the complex shows a total of 29 proton resonances between δ = 0 and 10 ppm. The methyl protons of the methoxy group and the methine proton appear as singlets as observed with the free ligand; however, for the methylene protons (NCH₂COO & NCH₂Ph) four doublet signals [NCH₂COO: 2.69 & 3.42 ppm, *J* = 15 Hz; NCH₂Ph: 3.74 & 3.94 ppm, *J* = 15 Hz] are observed, implying that each methylene proton became magnetically non-equivalent after complexation.

Electrochemical study

The redox properties of complexes 1–5 were studied by cyclic voltammetry in DMF under a dinitrogen atmosphere at room temperature. The redox potentials are measured *versus* the SCE. The cyclic voltammograms are presented in Fig. S33.† For complexes [Cu(L^R)(fla)] (1–4), during the cathodic scan an quasi-reversible reduction wave appears at *E*_{1/2} = −0.62 V for 1, −0.60 V for 2, −0.58 V for 3, and −0.56 V for 4, and can be assigned to the reduction of Cu(II) to Cu(I). However, we do not observe any metal centered reduction for Zn(II) complex 5, being a non-redox active metal ion. In the anodic scan all four Cu-fla complexes (1–4) show an irreversible oxidation wave at *E*_{pa} = 0.79 V for 1, 0.82 V for 2, 0.90 V for 3, and 0.96 V for 4, which may be assigned to one-electron oxidation from fla[−] to fla[•]. The fla[−]/fla[•] redox wave for complex 5 is observed at *E*_{pa} = 0.74 V. The *E*_{pa} values of present Cu-fla complexes 1–4 are much lower than those of the neutral N₄-ligand supported Cu-fla adduct reported in the literature;¹² however, these values are much higher than those of related Cu-fla compounds reported by Sun *et al.* having a carboxylate donor moiety in the ligand scaffold.¹³ For complexes 1–4, we observed an order of [Cu(L^{OMe})(fla)] (1) < [Cu(L^H)(fla)] (2) < [Cu(L^{Cl})(fla)] (3) < [Cu(L^{NO₂})(fla)] (4) for the *E*_{1/2} values of Cu^{II}/Cu^I and for the *E*_{pa} values of the fla[−]/fla[•] by changing the R substituents from an electron donating to an electron withdrawing group. In both cases, the potential values correlate linearly with the Hammett constants σ (Fig. 5). These findings indicate that the R substituents finely tune the electron density of the Cu(II) centre, and the electronic effect of the R groups is also propagated to the coordinated fla[−] ion *via* the benzyl group and Cu(II) ion “elec-

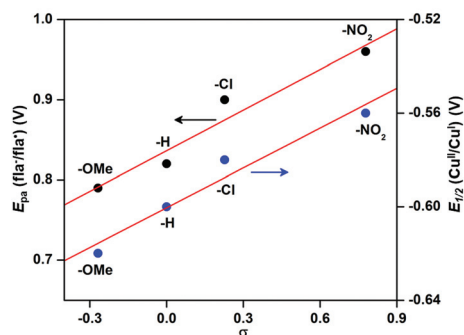


Fig. 5 Plots of *E*_{pa} of fla[−]/fla[•] and *E*_{1/2} of Cu^{II}/Cu^I of complexes 1–4 versus Hammett constants σ.

tron channel”. Therefore, the oxidation of the coordinated flavonolate is influenced by the nature of the substituent group in the supporting ligand L^R. The stronger the electron donating ability of R (−OMe > −H > −Cl > −NO₂) is, higher would be the electron density on the fla[−] ion, making the bound fla[−] ion more susceptible towards oxidation.

Oxygenative degradation of the ES model complexes – quercetin 2,4-dioxygenase-like activity

The oxygenative degradation of ES model complexes 1–5 was studied in DMF at 80 °C in the presence of dioxygen. Under aerobic conditions the substrate flavonolate undergoes the oxygenative ring-opening reaction to produce *o*-benzoysalicylic acid (HObs; *m/z* = 243.98 [M + 2H]⁺) with the release of carbon monoxide as primary products.²⁹ HObs undergoes further hydrolysis *via* a reaction with a small amount of water present in the solvent to produce salicylic acid (*m/z* = 139.01 [M + H]⁺) and benzoic acid (*m/z* = 121.05 [M − H]⁺). The salicylic acid and benzoic acid further react with solvent DMF under hot conditions over a prolonged reaction time (~10 h) to form the respective amide derivatives 2-hydroxy-*N,N*-dimethylbenzamide (*m/z* = 184.08 [M + H₂O + H]⁺) and *N,N*-dimethylbenzamide (*m/z* = 148.11 [M − H]⁺) (Fig. 6). The products were analysed by GC-MS and the product distributions are listed in Table S8.† A representative gas chromatogram for complex 2 and the illustrative mass spectra of the products from a few selected reactions are presented in Fig. S34.† At a shorter reaction time (~5 h) we could identify the formation of salicylic acid and benzoic acid as the major products from complex 2 by ¹H NMR spectroscopy as shown in Fig. S35.† Moreover, we could isolate and structurally characterize a salicylate bound copper (II) complex ([Cu(L^H)(sal)] (Fig. S36, CCDC 2112727†) from the post catalysis solution of 2. Therefore, from the above results it is apparent that all of our model complexes (1–5) exhibit enzyme-type reactivity.

To see the effect of R groups on their reactivity kinetic measurements with the copper(II)-flavonolate (1–4) complexes were performed at 80 °C in DMF. The kinetic studies were performed under pseudo first order conditions with a dioxygen saturated solution. The oxygenative degradation of the ES adducts was followed by monitoring the decrease of the absorption band (λ ~ 420 nm) due to the π → π* transition of

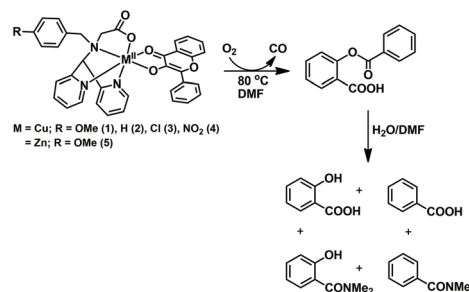


Fig. 6 Dioxygenation of the ES adducts (1–5) and their reaction products.

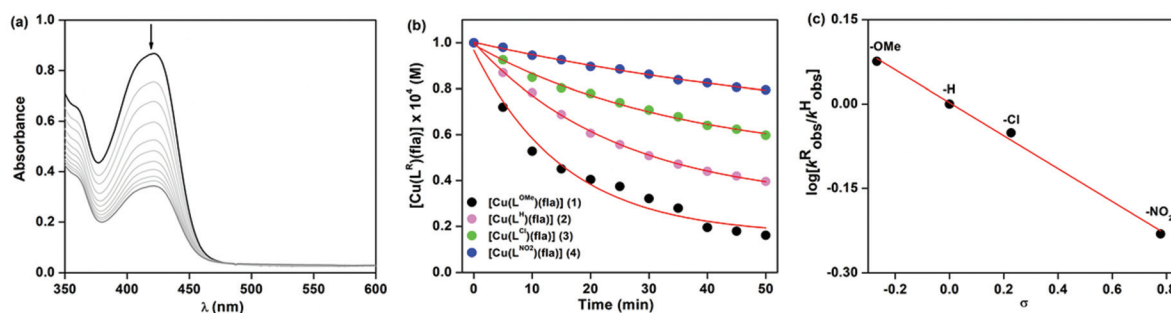


Fig. 7 (a) Spectral changes observed during the oxygenative degradation of **2** in the presence of dioxygen at 80 °C in DMF; (b) time course of the decay profile of the $[\text{Cu}(\text{L}^{\text{R}})(\text{fla})]$ complexes (**1–4**); (c) Hammett plot of the dioxxygenation of $[\text{Cu}(\text{L}^{\text{R}})(\text{fla})]$.

the coordinated flavonolate ligand over time. Here it should be noted that no degradation of any of the ES adducts was observed in the absence or at a low concentration of oxygen, implying that molecular dioxygen is necessary to bring about the oxygenative degradation reaction. The spectral change for the degradation reaction of **2** over time is presented in Fig. 7a for illustration. The time traces of the decay profiles for complexes **1–4** are presented in Fig. 7b. We consider apparently a first order decay profile for all complexes to calculate the pseudo first order rate constant values, $k_{\text{obs}} = 7.5 \times 10^{-2} \text{ min}^{-1}$ for (**1**), $6.3 \times 10^{-2} \text{ min}^{-1}$ for (**2**), $5.6 \times 10^{-2} \text{ min}^{-1}$ for (**3**) and $3.7 \times 10^{-2} \text{ min}^{-1}$ for (**4**). The $t_{1/2}$ values are determined to be 9.24 min, 11 min, 12.38 min, and 18.73 min for **1**, **2**, **3** and **4**, respectively. It is evident that the dioxxygenation reactivity of the bound flavonolate substrate of ES complexes **1–4** is highly influenced by the R substituents, following the order $1 > 2 > 3 > 4$. We obtain a nearly linear Hammett plot $[\log(k_{\text{obs}}^{\text{R}}/k_{\text{obs}}^{\text{H}})]$ vs. σ with slope $\rho = -0.30$ as shown in Fig. 7c. The negative Hammett constant is consistent with the generation of an electron-deficient flavonoxy radical (fla^{\cdot}) intermediate. Interestingly, this Hammett plot is just reverse with orders of the oxidation potential of $E_{\text{pa}}(\text{fla}^-/\text{fla}^{\cdot})$ of the Cu-fla adducts, as shown in Fig. 5. This result implies that the reactivity of the complexes depends on the oxidation potential of the bound flavonolate. The stronger electron donation to the Cu(II) centre by the R groups would increase the electron density on the metal centre. The enhanced electron density on the Cu(II) centre in turn results in a higher electron density on the flavonolate moiety, leading to the facile formation and greater stability of the flavonoxy radical (fla^{\cdot}) intermediate. Therefore, the observed trend of reactivity $1 > 2 > 3 > 4$ can be anticipated by considering the order of the electron donating ability of the R groups, $-\text{OMe} > -\text{H} > -\text{Cl} > -\text{NO}_2$. A similar substituent effect on the reactivity was also observed before with the $\text{Fe}^{17}/\text{Co}^{18a}/\text{Ni}^{19}$ analogues; however, to the best of our knowledge no such report is available in the literature with Cu-analogues. We have also estimated the rate of reactivity of the $[\text{Zn}(\text{L}^{\text{OMe}})(\text{fla})]$ (**5**) complex ($k_{\text{obs}} = 3.3 \times 10^{-2} \text{ min}^{-1}$; $t_{1/2} = 21 \text{ min}$). Although complex **1** and complex **5** have comparable $\text{fla}^-/\text{fla}^{\cdot}$ redox potential, we observed a much slower rate of reaction for **5** as compared to complex **1**. This may be due to the lower stability

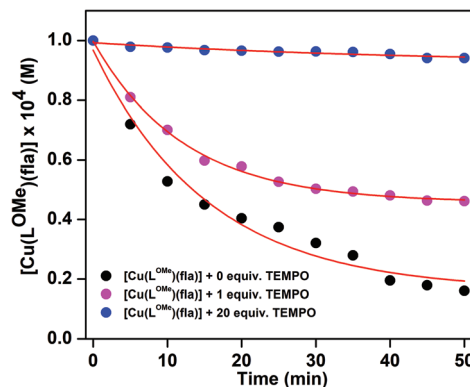


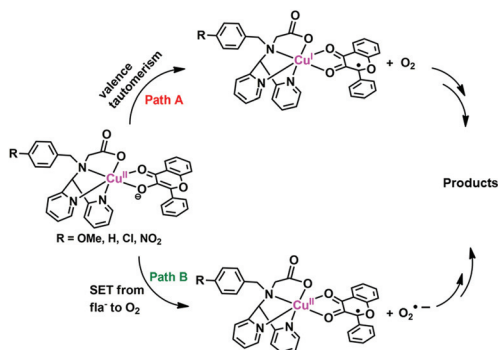
Fig. 8 Time traces of the oxygenative degradation of complex $[\text{Cu}(\text{L}^{\text{OMe}})(\text{fla})]$ (**1**) in the presence of TEMPO.

of the coordinated flavonoxy radical, presumably because of the lower degree of delocalization of the unpaired spin around the Zn(II) ion owing to the closed shell configuration.¹⁶

Discussion on a plausible mechanism

The above discussions point towards the fact that the dioxxygenation reactions of complexes **1–4** occur through a common pathway with the generation of a flavonoxy radical (fla^{\cdot}) at an initial step. The radical species is considered as an indispensable intermediate to promote the radical based degradation reaction. To validate this proposition, we studied the dioxxygenation reaction of complex **1** (the best performing compound in this series) in the presence of a free stable radical (2,2,6,6-tetramethylpiperidin-1-yl)oxyl (TEMPO) by UV-vis spectroscopy under previously described conditions. In the presence of one equivalent of TEMPO the degradation rate of the substrate reduced dramatically. Furthermore, when excess TEMPO (20 equivalents) was added only very slightly (<5%) degradation was observed (Fig. 8). The possible explanation of these findings could be that the initially generated flavonoxy radical was trapped by the TEMPO radical and thus the dioxxygenation reaction could not proceed further.

Two possible pathways as shown in Scheme 3 can generate the flavonoxy radical in complexes **1–4**. In path A, the valence



Scheme 3

tautomerism $\{[\text{Cu}^{\text{II}}(\text{fla}^-)] \leftrightarrow [\text{Cu}^{\text{I}}(\text{fla}^\bullet)]\}$, caused by one electron transfer from the substrate flavonolate anion (fla^-) to the Cu(II) ion, may lead to the generation of a flavoxy radical that triggers dioxygen activation with the involvement of Cu(I) as well. Such a pathway is believed to occur in the naturally occurring Cu²⁺-containing 2,4-QD enzymatic reaction.³ To verify the valence tautomerism phenomenon in the present synthetic model Cu-fla complexes we performed DFT calculations to get insight into the electronic structure of complexes 1–4. All structures were optimized in the doublet ground state. The spin density plots are depicted in Fig. S37† and the spin density values are tabulated in Table S9.† The calculations suggest that in all cases the oxidation state of the Cu centre can be assigned to +II and the flavonolate anion (fla^-) coordinated to the metal centre. The EPR spectra of all four complexes recorded in methanol at room temperature showed signals for the Cu(II) ion only, validating the calculated electronic structure of $[\text{Cu}^{\text{II}}(\text{fla}^-)]$. Furthermore, in the crystal structures of **1**·CH₂Cl₂·1.5H₂O and **2**·CH₂Cl₂·H₂O the bond distance of (fla)C–O_{3-hydroxide} in the respective complex (see Table 1) is typical of carbon–oxygen single bonds, attesting to the anionic nature of the bound substrate. Therefore, the above discussions pinpoint the $[\text{Cu}^{\text{II}}(\text{fla}^-)]$ electronic structure, predominantly at room temperature. However, the thermally induced valence tautomerism may lead to the generation of the $[\text{Cu}^{\text{I}}(\text{fla}^\bullet)]$ tautomer at elevated temperature. To verify such possibility, we recorded the electronic spectrum of complex **2** at 80 °C in DMF and compared the *d–d* band intensity (that originates due to Cu(II) ion) with that at room temperature. As can be seen in Fig. S38† we observed comparable *d–d* band intensities at both temperatures, thus, ruling out the thermally induced generation of the $[\text{Cu}^{\text{I}}(\text{fla}^\bullet)]$ tautomer even at 80 °C temperature. So, most probably the reaction does not proceed by path A for the present model complexes 1–4.³⁰

In another way, the reaction may proceed through path B, with a single-electron transfer (SET) from the flavonolate anion to O₂. To confirm the SET mechanism for the present Cu-fla complexes we use a redox-inactive Zn²⁺ complex $[\text{Zn}(\text{L}^{\text{OMe}})(\text{fla})]$ (**5**) and study its reactivity with dioxygen. As described above complex **5** also provides enzyme-type products. Therefore, it can be concluded that a direct one electron transfer from the

flavonolate to dioxygen occurs in the present synthetic model complexes to form a superoxide radical and a flavoxy radical. However, such an outer sphere electron transfer becomes feasible only at higher temperature, since no degradation was observed with any of the complexes at room temperature. To detect free O₂^{•-} we performed the EPR spin trapping experiment using 5,5-dimethyl-1-pyrroline-*N*-oxide (DMPO).^{31a} As shown in Fig. 9, an EPR signal ($g = 2.007$, $A = \sim 7$ G) corresponding to the species DMPO=O appeared, when 2 mM solution of $[\text{Cu}(\text{L}^{\text{H}})(\text{fla})]$ (**2**) in DMF reacted with 2 equivalents of DMPO in the presence of dioxygen at ~ 70 °C.^{31b} The superoxide radical reacted initially with DMPO to form a spin trapping adduct DMPO–OOH that further converted to DMPO=O under warm conditions. We also performed a nitro blue tetrazolium (NBT²⁺) test to detect the superoxide ion. When complex $[\text{Cu}(\text{L}^{\text{H}})(\text{fla})]$ (**2**) was treated with an excess of NBT²⁺ in the presence of dioxygen under warm conditions, a band at 510 nm in the UV-vis spectrum (Fig. S39†) was observed due to a monoformazan species (MF⁺), indicating that complex **2** reacted with dioxygen to produce superoxide, which then reduced NBT²⁺ to MF⁺.^{31c} Thus, both the experiments evidently validate the *in situ* generation of free superoxide during the reaction.

To explore the dioxygenation pathway we performed a computational study with **2**. The energy profile for the dioxygenation reaction is shown in Fig. 10. The optimized structures of various transition states and intermediates are depicted in Fig. S40.† The Mulliken spin density values are tabulated in Table S10.† The calculated coordinates are listed from Tables S11 to S20 in the ESI.† The absolute energies are tabulated in Table S21.† As can be seen from Table S10,† throughout the reaction copper remains in the +II oxidation state. The energy of the reactants (⁴R) is defined by considering the sum of the energies of triplet O₂ (³O₂) and doublet complex **2**. The reaction proceeds through the generation of the flavoxy radical and superoxide in ⁴TS1 via single-electron transfer (SET) from flavonolate to O₂, followed by C(2)–O_p bond formation to generate intermediate ⁴I1. The activation energy of ⁴TS1 relative to

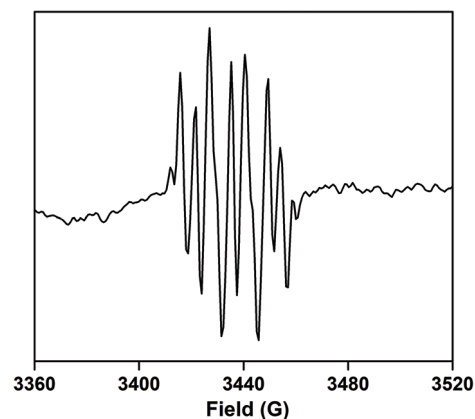


Fig. 9 EPR spectrum of the reaction of **2** with DMPO under O₂ in DMF (microwave frequency ≈ 9.65 GHz; the spectrum was measured at 298 K).

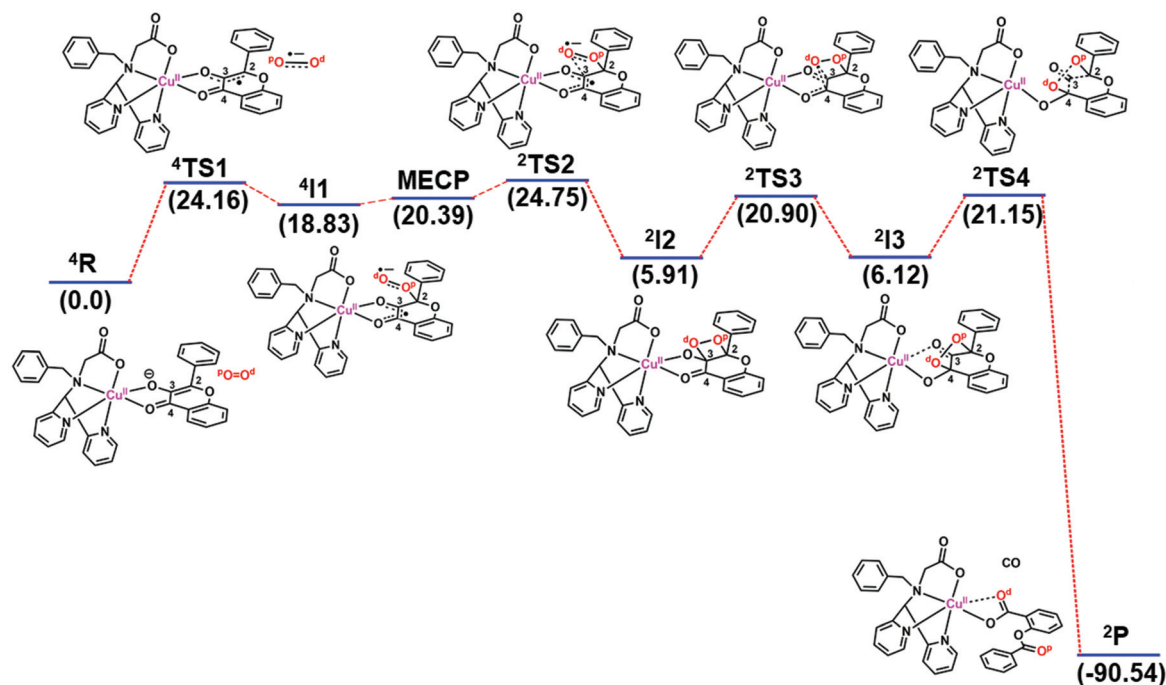


Fig. 10 Reaction coordinate for the dioxygenation reaction with complex $[\text{Cu}^{\text{II}}(\text{L}^{\text{H}})(\text{fla})]$ (**2**). The relative energies of various states are presented in parenthesis in kcal mol^{-1} (R = reactants; TS = transition state; I = intermediate; MECP = minimum energy crossing point; P = product). The superscripts indicate the spin states.

^4R is computed to be $24.16 \text{ kcal mol}^{-1}$. The relative energy of $^4\text{I1}$ is $18.83 \text{ kcal mol}^{-1}$, which is close to $^4\text{TS1}$, implying that $^4\text{I1}$ is an unstable and reactive intermediate. In the next step intersystem crossing takes place through a transition state $^2\text{TS2}$ to generate a relatively stable 1,2-dioxetane intermediate ($^2\text{I2}$) at the doublet state. The ring-closer reaction involving $\text{C}(2)\text{-O}_d\text{-O}_p\text{-C}(3)$ takes place *via* a singlet $\text{C3}(\uparrow)\cdots\text{superoxide}(\downarrow)$ radical coupling pathway. In the preceding step $^2\text{I2}$ converts readily to the endoperoxide intermediate ($^2\text{I3}$) *via* $^2\text{TS3}$. Once endoperoxide is formed the cleavage of $\text{O}_p\text{-O}_d$, C2-C3 , and C3-C4 bonds *via* $^2\text{TS4}$ leads to the generation of the *o*-benzoylsalicylato-copper(II) complex along with carbon monoxide as products. The product formation is highly exothermic that provides the driving force to proceed reaction in the forward direction. The computed pathway corroborates well with that reported for $[\text{Cu}(\text{idpa})(\text{fla})]$ in the literature.³² The energy profile diagram suggests that the single-electron transfer followed by the formation of the 1,2-dioxetane intermediate is likely to be the rate-determining step. The dependence of the dioxygenation reactivity on the oxidation potential of $\text{fla}^-/\text{fla}^{\cdot}$ in complexes **1–4** validates this prediction.

Summary and conclusions

In the present work, we have demonstrated the syntheses and characterization of a series of copper(II)-flavonolate complexes $[\text{Cu}^{\text{II}}(\text{L}^{\text{R}})(\text{fla})]$ $\{\text{R} = -\text{OMe}$ (**1**), $-\text{H}$ (**2**), $-\text{Cl}$ (**3**), $-\text{NO}_2$ (**4**) $\}$, supported with a carboxylate-containing tetradentate N_3O donor

ligand, as structural and functional ES models of the Cu^{2+} -containing 2,4-QD enzyme. Complexes **1–4** are synthesized from the corresponding acetate-bound copper(II) complexes, $[\text{Cu}^{\text{II}}(\text{L}^{\text{R}})(\text{OAc})]$ by a reaction with 3-hydroxyflavone in the presence of a base under inert conditions. In the presence of dioxygen the ES model complexes **1–4** exhibit enzyme-type dioxygenase activity at 80°C in DMF. The reactivity rate is highly governed by the electron donating properties of R substituents, following the order $-\text{OMe}$ (**1**) $>$ $-\text{H}$ (**2**) $>$ $-\text{Cl}$ (**3**) $>$ $-\text{NO}_2$ (**4**). Stronger the electron donation, lower the oxidation potential of $\text{fla}^-/\text{fla}^{\cdot}$ couple and thereby, higher the rate of the dioxygenation reaction. The finding of the linear Hammett correlation $[\log(k_{\text{obs}}^{\text{R}}/k_{\text{obs}}^{\text{H}})]$ *vs.* σ with a negative slope is consistent with the generation of an electron-deficient flavonoxyl radical (fla^{\cdot}) intermediate. Based on the experimental and theoretical studies we argued over a single-electron transfer (SET) from flavonolate to O_2 rather than valence tautomerism to generate the reactive fla^{\cdot} radical intermediate. This was further verified by observing enzyme-type product formation with a redox-inactive Zn^{2+} complex $[\text{Zn}(\text{L}^{\text{OMe}})(\text{fla})]$ (**5**). The present results suggest that the synthetic model complexes might react differently from the naturally occurring enzyme, depending on the overall electronic impact exerted by the supporting ligand.

Author contributions

N. P. synthesized and characterized all the complexes, performed all experimental works, and analysed the data. S. D.

and A. A. contributed to the DFT calculations. S. M. conceived the project, analysed the data and wrote the paper.

Conflicts of interest

There are no conflicts to declare.

Acknowledgements

S. M. gratefully acknowledges the Council of Scientific and Industrial Research, Government of India [Grant 01(3052)/21/EMR-II]; Science and Engineering Research Board (SERB), Government of India (Ref.: EMR/2015/001136); DST-INSPIRE Faculty award, Government of India (Ref.: DST/INSPIRE Faculty Award/IFA12-CH-72); ISIRD start-up research grant, IIT Kharagpur (Ref.: IIT/SRIC/CHY/SMR/2015-16/60) for the financial support to establish the laboratory. N. P. thanks the IIT Kharagpur for a Ph.D. fellowship. S. D. thanks the University Grants Commission (UGC) for a Ph.D. fellowship. We thank the Department of Science and Technology (DST), Government of India, under the DST-FIST programme for the NMR (SR/FST/CSII-026/2013) facility. We thank the Central Research Facility, IIT Kharagpur, for providing access to the EPR and HRMS instruments. We also thank the Department of Chemistry, IIT Kharagpur, for providing infrastructural and other major instrumental facilities (X-ray, NMR, GC-MS, HRMS *etc.*). We are thankful for the resources of the Supercomputing facility at IIT Kharagpur established under the National Supercomputing Mission (NSM), Government of India and supported by the Center for Development of Advanced Computing (CDAC), Pune.

Notes and references

- E. Wollenweber, in *Flavonoids: Advances in Research*, ed. J. B. Harborne and T. J. Mabry, Chapman & Hall, London, 1982.
- F. Fusetti, K. H. Schröter, R. A. Steiner, P. I. van Noort, T. Pijning, H. J. Rozeboom, K. H. Kalk, M. R. Egmond and B. W. Dijkstra, *Structure*, 2002, **10**, 259–268.
- R. A. Steiner, K. H. Kalk and B. W. Dijkstra, *Proc. Natl. Acad. Sci. U. S. A.*, 2002, **99**, 16625–16630.
- I. M. Kooter, R. A. Steiner, B. W. Dijkstra, P. I. van Noort, M. R. Egmond and M. Huber, *Eur. J. Biochem.*, 2002, **269**, 2971–2979.
- R. A. Steiner, I. M. Kooter and B. W. Dijkstra, *Biochemistry*, 2002, **41**, 7955–7962.
- (a) J. Kaizer, É. Balogh-Hergovich, M. Czaun, T. Csay and G. Speier, *Coord. Chem. Rev.*, 2006, **250**, 2222–2233; (b) J. S. Pap, J. Kaizer and G. Speier, *Coord. Chem. Rev.*, 2010, **254**, 781–793.
- (a) É. Balogh-Hergovich, J. Kaizer, J. Pap, G. Speier, G. Huttner and L. Zsolnai, *Eur. J. Inorg. Chem.*, 2002, 2287–2295; (b) É. Balogh-Hergovich, J. Kaizer and G. Speier, *Inorg. Chim. Acta*, 1997, **256**, 9–14; (c) L. Barhács, J. Kaizer, J. Pap and G. Speier, *Inorg. Chim. Acta*, 2001, **320**, 83–91; (d) J. Kaizer, S. Góger, G. Speier, M. Réglér and M. Giorgi, *Inorg. Chem. Commun.*, 2006, **9**, 251–254; (e) É. Balogh-Hergovich, J. Kaizer and G. Speier, *J. Mol. Catal. A: Chem.*, 2000, **159**, 215–224; (f) W. E. Lynch, D. Nivens, B. Quillian, C. W. Padgett, A. Petrillo, N. Peek and J. A. Stone, *J. Mol. Struct.*, 2019, **1185**, 99–106.
- (a) I. Lippai, G. Speier, G. Huttner and L. Zsolnai, *Acta Crystallogr., Sect. C: Cryst. Struct. Commun.*, 1997, **53**, 1547–1549; (b) É. Balogh-Hergovich, J. Kaizer, G. Speier, V. Fülöp and L. Párkányi, *Inorg. Chem.*, 1999, **38**, 3787–3795; (c) É. Balogh-Hergovich, J. Kaizer, G. Speier, G. Huttner and L. Zsolnai, *Inorg. Chim. Acta*, 2000, **304**, 72–77; (d) É. Balogh-Hergovich, J. Kaizer, G. Speier, G. Huttner and A. Jacobi, *Inorg. Chem.*, 2000, **39**, 4224–4229; (e) J. Kaizer, J. Pap, G. Speier and L. Párkányi, *Eur. J. Inorg. Chem.*, 2004, 2253–2259.
- É. Balogh-Hergovich, J. Kaizer and G. Speier, *J. Mol. Catal. A: Chem.*, 2003, **206**, 83–87.
- A. Y. S. Malkhasian, M. E. Finch, B. Nikolovski, A. Menon, B. E. Kucera and F. A. Chavez, *Inorg. Chem.*, 2007, **46**, 2950–2952.
- Y.-J. Sun, P. Li, Q.-Q. Huang, J.-J. Zhang and S. Itoh, *Eur. J. Inorg. Chem.*, 2017, 1845–1854.
- K. Grubel, K. Rudzka, A. M. Arif, K. L. Klotz, J. A. Halfen and L. M. Berreau, *Inorg. Chem.*, 2010, **49**, 82–96.
- Y.-J. Sun, Q.-Q. Huang, T. Tano and S. Itoh, *Inorg. Chem.*, 2013, **52**, 10936–10948.
- A. Matuz, M. Giorgi, G. Speier and J. Kaizer, *Polyhedron*, 2013, **63**, 41–49.
- Y.-J. Sun, Q.-Q. Huang, P. Li and J.-J. Zhang, *Dalton Trans.*, 2015, **44**, 13926–13938.
- S. Hoof and C. Limberg, *Inorg. Chem.*, 2019, **58**, 12843–12853.
- Y.-J. Sun, Q.-Q. Huang and J.-J. Zhang, *ACS Omega*, 2017, **2**, 5850–5860.
- (a) Y.-J. Sun, Q.-Q. Huang and J.-J. Zhang, *Inorg. Chem.*, 2014, **53**, 2932–2942; (b) Y.-J. Sun, Y.-F. Liu, J.-J. Zhang and Y.-Q. Li, *ChemistrySelect*, 2019, **4**, 13974–13982.
- Y.-J. Sun, Q.-Q. Huang and J.-J. Zhang, *Dalton Trans.*, 2014, **43**, 6480–6489.
- J. Chang, S. Plummer, E. S. F. Berman, D. Striplin and D. Blaich, *Inorg. Chem.*, 2004, **43**, 1735–1742.
- (a) G. M. Sheldrick, *Acta Crystallogr., Sect. A: Found. Adv.*, 2015, **71**, 3–8; (b) L. J. Farrugia, *J. Appl. Crystallogr.*, 2012, **45**, 849–854; (c) L. J. Farrugia, *WINGX Version 2021.2. An Integrated Systems of Windows programs for the solution, Refinement and Analysis of Single-Crystal X-ray Diffraction Data*, School of Chemistry, University of Glasgow, Glasgow, UK, 2021.
- (a) F. Neese, *Wiley Interdiscip. Rev.: Comput. Mol. Sci.*, 2018, **8**, e1327; (b) J.-D. Chai and M. Head-Gordon, *Phys. Chem. Chem. Phys.*, 2008, **10**, 6615–6620; (c) F. Weigend and R. Ahlrichs, *Phys. Chem. Chem. Phys.*, 2005, **7**, 3297–3305; (d) F. Neese, F. Wennmohs, A. Hansen and U. Becker,

- Chem. Phys.*, 2009, **356**, 98–109; (e) A. Klamt and G. Schüürmann, *J. Chem. Soc., Perkin Trans. 2*, 1993, 799–805; (f) K. Fukui, *J. Phys. Chem.*, 1970, **74**, 4161–4163.
- 23 A. W. Addison, T. N. Rao, J. Reedijk, J. van Rijn and G. C. Verschoor, *J. Chem. Soc., Dalton Trans.*, 1984, 1349–1356.
- 24 (a) L. Jurd and T. A. Geissman, *J. Org. Chem.*, 1956, **21**, 1395–1401; (b) L. Barhács, J. Kaizer and G. Speier, *J. Org. Chem.*, 2000, **65**, 3449–3452.
- 25 G. B. Deacon and R. J. Phillips, *Coord. Chem. Rev.*, 1980, **33**, 227–250.
- 26 R. Mukherjee, Copper, in *Comprehensive Coordination Chemistry II: From Biology to Nanotechnology*, ed. J. A. McCleverty, T. J. Meyer and D. E. Fenton, Elsevier/Pergamon, Amsterdam, 2004, vol. 6, pp. 747–910.
- 27 (a) G. S. Uscumlic, D. Z. Mijin, N. V. Valentic, V. V. Vajs and B. M. Susic, *Chem. Phys. Lett.*, 2004, **397**, 148–153; (b) G. Barcenas, A. Biaggne, O. A. Mass, C. K. Wilson, O. M. Obukhova, O. S. Kolosova, A. L. Tatarets, E. Terpetschnig, R. D. Pensack, J. Lee, W. B. Knowlton, B. Yurke and L. Li, *RSC Adv.*, 2021, **11**, 19029–19040.
- 28 S. Stoll and A. Schweiger, *J. Magn. Reson.*, 2006, **178**, 42–55.
- 29 We did not carry out the analysis of CO release during reaction as DMF has a tendency to decompose slightly at elevated temperature to yield dimethylamine and CO, which would lead false interpretation.
- 30 It may be noted that if the existence probability of the copper(i)-fla[•] intermediate is very low (not detectable by ordinary spectroscopic methods), but its reactivity toward dioxygen is much higher than that of copper(ii)-fla, the mechanism involving the copper(i)-fla[•] intermediate (path A in Scheme 3) cannot be completely excluded.
- 31 (a) M. Velayutham, C. Hemann and J. L. Zweier, *Free Radical Biol. Med.*, 2011, **51**, 160–170; (b) T. Ueda, H. Kitagishi and K. Kano, *Inorg. Chem.*, 2014, **53**, 543–551; (c) B. H. J. Bielski, G. G. Shiue and S. Bajuk, *J. Phys. Chem.*, 1980, **84**, 830–833.
- 32 T. Numata, T. Saito, T. Kawakami, S. Yamanaka and M. Okumura, *Polyhedron*, 2017, **136**, 45–51.